POU6F2 mutation identified in humans with pubertal failure shifts isoform formation and alters GnRH transcript expression.

Hyun-Ju Cho,[1,‡] Fatih Gurbuz,[2,‡] Maria Stamou[3], Leman Damla Kotan,[2] Stephen Matthew Farmer,[1] Sule Can,[4] Miranda Faith Tompkins[1], Jamala Mammadova,[5] S. Ayca Altincik,[6] Cumali Gokce,[7] Gonul Catli,[4] Fuat Bugrul,[8] Keenan Bartlett,[1] Ihsan Turan,[2] Ravikumar Balasubramanian[3], Bilgin Yuksel,[2] Stephanie B. Seminara[3], Susan Wray, [1, ‡,*] and A. Kemal Topaloglu,[9,10, ‡,*]

[1]Cellular and Developmental Neurobiology Section, National Institute of Neurologic Disorders and Stroke, National Institutes of Health; Bethesda, Maryland, 20892, USA.

[2]Division of Pediatric Endocrinology, Cukurova University, Faculty of Medicine. Adana, 01330, Turkey.

[3]Harvard Reproductive Sciences Center, The Reproductive Endocrine Unit and The Endocrine Unit of the Department of Medicine, Massachusetts General Hospital, Boston, MA, USA.

[4]Division of Pediatric Endocrinology, Health Sciences University, İzmir Tepecik Training and Research Hospital; İzmir, 35020, Turkey.

[5]Division of Pediatric Endocrinology, Ondokuz Mayis University, Faculty of Medicine; Samsun, 55139, Turkey.

[6]Division of Pediatric Endocrinology, Pamukkale University, Faculty of Medicine; Denizli, 20070, Turkey.

[7]Division of Endocrinology, Mustafa Kemal University, Faculty of Medicine; Hatay, Turkey.

[8]Division of Pediatric Endocrinology, Selcuk University, Faculty of Medicine, Konya, 42130, Turkey

[9]Department of Pediatrics, Division of Pediatric Endocrinology, University of Mississippi Medical Center, Jackson, Mississippi, 39216, USA

[10]Department of Neurobiology and Anatomical Sciences, University of Mississippi Medical Center, Jackson, Mississippi, 39216, USA

[‡]These authors contributed equally to this work.

[*]Corresponding authors

Susan Wray

wrays@ninds.nih.gov

+1) 301-496-6646

A. Kemal Topaloglu

ktopaloglu@umc.edu

+1) 601-984-5216

ABSTRACT

Idiopathic hypogonadotropic hypogonadism (IHH) is characterized by absent pubertal development and infertility, often due to gonadotropin-releasing hormone (GnRH) deficits. Exome sequencing of two independent cohorts of IHH patients identified 12 rare missense variants in *POU6F2*. *POU6F2* encodes two distinct isoforms. In mouse, pituitary and gonads expressed both isoforms, but only isoform1 was detected in GnRH cells. Although the function of isoform2 is well known, using bioinformatics and cells assays on a human-derived GnRH cell line, we demonstrate isoform1 can also act as a transcriptional regulator, decreasing *GNRH1* expression. The impact of two *POU6F2* variants (MT1 and MT2) was then examined. MT1, but not MT2, reduced transcriptional activity of either isoform, preventing Hes5 promoter activation by isoform2 and repression of GnRH transcripts by isoform1. GnRH transcription increases as the cells migrate into the brain. Augmentation earlier can disrupt normal GnRH cell migration, consistent with POU6F2 variants contributing to IHH pathogenesis.

INTRODUCTION

Idiopathic Hypogonadotropic Hypogonadism (IHH) is a rare genetic disorder characterized by complete or partial pubertal failure caused by gonadotropin-releasing hormone (GnRH) deficiency. According to olfactory function, IHH is divided into two major forms, normal sense of smell (normosmic IHH, nIHH) and inability to smell, anosmia, defined as Kallmann syndrome (KS). Although nearly 50 genes have been reported to be associated with IHH(Howard & Dunkel, 2019; Louden et al., 2021), they account for only 50% of all cases indicating that other associated genes remain to be discovered. Delineating new genes involved in the development and/or function of GnRH neurons is relevant for understanding the basis of IHH pathogenesis in humans. We identified missense variants in *POU6F2* in IHH patients. Most POU-family members have known roles as transcriptional regulators, with many of them controlling cell type-specific differentiation pathways(Andersen & Rosenfeld, 2001; Kim, Han, Kim, & Schöler, 2021). Several POU domain-containing gene products modulate development, expression, and function of GnRH neurons(Leclerc & Boockfor, 2005; Wierman et al., 1997; Wolfe, Kim, Tobet, Stafford, & Radovick, 2002). POU6F2 has two distinct isoforms, with isoform2 being a known transcriptional regulator while the function of isoform1 is unclear. In this communication, we present evidence that POU6F2 isoform1 can also function as a transcription factor repressing *GnRH1* expression and that one of the POU6F2 variants identified alters isoform splicing and reduced transcriptional activity of either isoform. Together, these data are consistent with mutations in *POU6F2* contributing to the pathogenesis of IHH.

RESULTS

Twelve rare missense *POU6F2 variants* (HGNC: 21694) in 15 patients from 12 unrelated families were identified. The pedigrees with clinical phenotypical features are depicted in Figure 1 and Table 1. Molecular genetic characteristics of the variants are shown in Table 2. Three POU domain variants (MT1,MT2,MT8) reside in regions necessary for proper protein function or dimerization (Figure 2A). The remaining variants (MT3-7) are in the transactivation domain. Ten of the 12 variants had CADD scores >20 and were either not seen in the largest reference population database (gnomAD) or occurred at an extremely rare minor allele frequency <0.0005. However, MT2 was found to be significantly more common in the newly published Turkish Variome at 0.002(Kars et al., 2021) (Table 2). No variant was previously reported in ClinVar. All were classified as variants of uncertain significance (VUS), except MT4 and MT7 which were categorized as 'likely pathogenic" by ACMG/AMP classification(Richards et al., 2015). However, Polyphen-2(Adzhubei et al., 2010) and SIFT(Kumar, Henikoff, & Ng, 2009), two well-validated *in silico* prediction programs indicated most of these variants to be harmful (Table 2).

In Family-A, three brothers born from a consanguineous union presented with pubertal impairment implicating an autosomal recessive mode of inheritance. All three brothers carried a homozygous mutation (p.Gly601Arg). The two younger siblings had complete IHH. The oldest sibling received monthly testosterone injections at 15yrs because of pubertal delay and by age 17 had started puberty. As different from his brothers, the milder reproductive phenotype of this patient is consistent with constitutional delay in growth and puberty, also known as self-limited delayed puberty. It has been previously observed that variants in IHH genes can also cause self-limited delayed puberty, even sometimes within the same kindreds, indicating self-limited delayed puberty shares an underlying pathophysiology with IHH(Saengkaew et al., 2021; Zhu et al., 2015). The pattern of inheritance in Family-A is clearly autosomal recessive (Fig 1). MT8 (p.Arg494Trp)

in Family-I arose *de novo*. A perfect segregation of an autosomal recessively inherited mutation with pubertal impairment phenotype in multiplex families such as in Family-A was given high scores in the Clinical Genome Resource (ClinGen) framework to define and evaluate the validity of gene-disease pairs across a variety of Mendelian disorders(Strande et al., 2017). Likewise, the *de novo* variant in Family-I provides strong genetic evidence supporting causality of mutations in novel gene-disease associations(Strande et al., 2017).

The inheritance in the other pedigrees is consistent with autosomal dominant with variable penetrance and expressivity, a phenomenon commonly observed in IHH(Bouilly et al., 2018; Louden et al., 2021; Xu et al., 2017). The male patients in Family-B, Family-H, and Family-L had cryptorchidism, indicating severe congenital hypogonadism. In congenital IHH, fetal pituitary gonadotropin secretion is low, leading to inadequate fetal serum testosterone levels. As the testicular descent and growth of phallus are androgen-dependent during fetal and neonatal periods, boys with severe IHH present with micropenis, cryptorchidism, and hypospadias at birth(Pitteloud et al., 2002). The younger patient in Family-B was diagnosed with IHH based on hypogonadal features plus prepubertal gonadotropins and testosterone level at two months of age, a time window known as minipuberty, a poorly understood transient activation of the hypothalamic-pituitary-gonadal (HPG) axis between 2-6 months of age. With an appropriate physical examination and laboratory findings, it is possible to make a diagnosis of IHH during this very early window of human life(Renault et al., 2020).

In Family-C the 17yr female proband has the same mutation as the one in Family-B. In addition, she carries a distinct rare variant in another POU-family gene, *POU6F1* (See Discussion for detailed assessment). The probands in the remaining eight families (other than in families A, B, C and H) had variants in the non-POU domain part of the gene (Figure 2), the function of which

remain poorly defined. We did not perform functional studies on these non-POU domain variants. However, these extremely rare variants were predicted to be deleterious by *in silico* analysis (see Table 2).

Three mutations (MT1, MT2 and MT8) are located in the POU-specific domain (POU_S, MT8), the linker region between the POU_S and the POU-homeodomain (POU_H, MT1) or in the POU_H (MT2, Figure 2A)(Fiorino et al., 2016; Zhou, Yoshioka, & Nathans, 1996). R494(MT8) is in the first alpha helix of the POU_S domain which is highly conserved in orthologs and conserved among paralogs as positively charged amino acids R or K. As such a mutation changing R to W may alter structure of this alpha helix. However, data from other POU-family members indicate that it is residues of the third alpha helix in the POU_S domain that are involved in hydrogen bonding with DNA base pairs(Pereira & Kim, 2009). As such we performed *in silico analysis* (Supplementary Table 1, Supplementary Figure 2), but not functional studies of MT8. In contrast to MT8, R601(MT1) and N629(MT2) are located at/or close to the edge of alpha helixes that compose the POU_H domain, and these are less conserved among paralogs but well conserved in orthologs. Notably, MT1 and MT2 are on exon11 which is alternatively spliced and distinguishes the two POU6F2 isoforms that have been identified (Figure 2).

Pou6f2 isoforms are differentially expressed in mouse hypothalamic-pituitary-gonadal axis tissue

To determine which isoform might be pertinent to patients exhibiting IHH, the expression of POU6F2 isoforms in HPG axis relevant tissues was performed on mouse tissue using RT-PCR (Figure 3). *Pou6f2* is well conserved between human and mouse, except with respect to the 5' UTR, which is located on exon1 and exon2 in human, while mouse *Pou6f2* has a shorter 5' UTR with its

coding region starting from exon1 (Compare Figure 2A, human and 3A, mouse). Thus, mouse *Pou6f2* has 9 exons which correspond to exon3-11 in the human. To date, only one *Pou6f2* mRNA sequence has been catalogued in NCBI, however, the alternative splicing of the last exon was analyzed in mouse retina cDNA and revealed the presence of both isoform1 and 2(Fiorino et al., 2016). In brain, pituitary and gonads (Figure 3B), both isoforms were present, though expression of isoform1 was more abundant than isoform2. Analysis of primary GnRH cells (Figure 3C, N=5) with primers that detect both isoform1 and isoform2, showed only isoform1 transcript present in 2 of the tested single GnRH cells. To ensure that isoform2 was not being missed due to low expression, the samples were rescreened with isoform2 only specific primers (Figure 3C). After 45 cycles of amplification, no isoform2 transcripts were detected in any of the GnRH cells, though brain cDNA was positive. Thus, in primary GnRH cells isoform1 is the predominant *Pou6f2* isoform that is expressed.

POU6F2 modeling

Previous studies have shown that POU6F2 isoform2 binds to divergent POU and combined SOX/POU DNA sequences and mediates transcriptional activity while isoform1 binds poorly to these sequences and shows little transcriptional activity(Fiorino et al., 2016; Zhou et al., 1996). *In silico* analysis was used on the two isoforms to establish the validity of our modeling. Although POU6F2 is yet to be crystallized, a closely related paralog human POU6F1 has been crystallized bound to an octamer motif(Pereira & Kim, 2009) which increases the accuracy of homology modeling(Haddad, Adam, & Heger, 2020). C-I-TASSER produced structures for POU6F2 isoform1 and 2 (Figure 2B) using the POU6F1 crystal template with good resolution (PDB code: 3D1N; resolution=2.51 Å). The POU domains for each POU6F2 isoform were in the same fold as

168 POU6F1 (TM-score$_{iso1}$=0.66, RMSD$_{iso1}$=1.03; TM-score$_{iso2}$=0.80, RMSD$_{iso2}$=0.81). Highly
169 variant N-terminal domains upstream of the POU domains were not detected in the original
170 POU6F1 crystal and were disordered in POU6F2 structures and thus were omitted in downstream
171 structural experiments. Previous experiments indicated that only isoform2 binds to OCT1
172 consensus DNA(Zhou et al., 1996). w3DNA was used to predict the structure of the human OCT1
173 DNA consensus sequence (5'-$A_1T_2G_3C_4A_5A_6A_7T_8$-3'), and HDOCK predicted a more favorable
174 scoring function of binding for isoform2 (-303.26au) compared to isoform1 (-258.88au). The
175 predicted binding mode showed that isoform2 POU$_S$ binds to 5'- $A_1T_2G_3C_4$-3' and POU$_H$ to 5'-
176 $A_5A_6A_7T_8$-3' by embracing both faces of dsDNA, whereas isoform1 did not (Figure 3D). This is
177 consistent with literature showing that isoform2 can bind these octamer consensus sequences,
178 whereas isoform1 cannot(Zhou et al., 1996).
179
180 **POU domain mutation identified in IHH patients alters splicing preference of human exon11**
181 Alternative splicing of *POU6F2* has been identified in human retina cDNA(Zhou et al., 1996), but
182 the proportion of the mRNA isoforms derived from those splicing events is not well known. The
183 most studied splicing event is on exon11, which distinguishes isoform1 and isoform2. Two
184 mutations (MT1 and MT2) identified in this study reside in exon11 which can affect both isoforms
185 (Figure 2A). To predict the possible effect of both mutations on splicing of exon11 and isoform
186 expression, *in silico* splicing analysis was performed using online prediction programs. Both
187 mutations are predicted to affect splicing by 3 out of 4 prediction programs (Figure 4A).
188 To directly analyze the possible splicing changes on exon11, *in vitro* splicing assays were
189 performed by introducing human exon11 into pSPL3 minigene plasmids in between two artificial
190 exons designed to be spliced into a single mRNA (Figure 4B). Plasmids were transfected into

HEK293 cells, cultured for 2 days and processed mRNAs obtained. RT-PCR using SD6F (forward primer on exonA) and E11R (reverse primer on POU6F2 exon11) showed two different sized bands from both WT and mutant sequences but not pSPL3 mock (Figure 4C). The upper band (508 bp) is spliced from exonA (92bp) to exon11 (416bp) via the first splicing acceptor site (SA1) forms isoform1. The smaller band (400bp) is spliced from exonA to exon11 (308bp) via the second splicing acceptor site (SA2) forms isoform2. The DNA sequence of each band was confirmed by TA-cloning of PCR products and plasmid sequencing (Figure 4D). Neither new splicing variants nor absence of normal splicing variants were observed from either mutant sequence. However, the band intensities of the isoforms changed with the introduction of MT1. In WT, the isoform1 splicing band was stronger than the isoform2 splicing band (Figure 4C). Introduction of MT1 reversed this relationship, with the isoform2 band now stronger, though isoform1 was still present (Figure 4C). To obtain a better measurement of the isoforms, qPCR analysis was performed using primers specific for each isoform. The ratio of isoform2/1 was calculated and represented as a relative value compared to WT (Figure 4E). MT1 resulted in a significant increase in the ratio of isoform2/1 (~1.6-fold higher than WT) while the ratio obtained for mutation 2 (MT2) was similar to WT. No significant differences were observed with or without cycloheximide treatment suggesting that these spliced mRNAs were stable from nonsense-mediated decay. To further evaluate the potential effects of MT1 and MT2 on isoform1 and isoform2, functional evaluation of the mutant proteins was performed using computational modeling and *in vitro* transcriptional assays.

Functional analysis of POU6F2 isoform2 as a known transcription factor

213 POU6F2 isoform2 is a known transcriptional regulator(Fiorino et al., 2016). To examine the
214 alterations induced by MT1 and MT2 on isoform2 (Figure 5A), DynaMut and CABS-flex were
215 used to determine changes in protein structure. DynaMut predicted that both mutations stabilized
216 isoform2 folding ($\Delta\Delta G_{MT1}$=0.956; $\Delta\Delta G_{MT2}$=0.211, Figure 5B). Protein flexibility dictates not only
217 a protein's function but also its ability to respond to stochastic environmental changes(Teilum,
218 Olsen, & Kragelund, 2011). CABS-flex revealed that isoform2 protein flexibility was largely
219 diminished by both mutations (P=0.0001, figure 5B). SAMPDI was then used to predict changes
220 in the affinity of isoform2, in the setting of either MT1 and MT2, for the known OCT1 DNA
221 consensus. Both mutations were predicted to destabilize this interaction. In sum, *in silico* analysis
222 predicted that the MT1 and MT2 found in IHH patients would be deleterious to the intrinsic
223 properties of the POU6F2 isoform2, including both its protein flexibility and affinity for DNA.
224 To directly evaluate the transcriptional activity of WT and mutant isoform2 POU6F2
225 proteins, *in vitro* transcription assays were performed using a DsRed reporter under the *Hes5*
226 promoter (760bp, Figure 5C). *Hes5* is known to be upregulated by isoform2 overexpressed in
227 HEK293 cells(Fiorino et al., 2016) and the promoter sequence used for assay includes two
228 predicted POU protein binding sequences (5'-AAGCAAAT-3' and 5'-ATGCTAAT-3'; predicted
229 by PROMO v3.0.2). Isoform1 (non-*Hes5* DNA binding control) or isoform2 (DNA-binding)
230 expression vectors were co-transfected into HEK293FT cells with Hes5p-DsRed plasmids; then
231 the expression of DsRed was analyzed by Western blot assay. Isoform2 showed a significant
232 increase in DsRed expression (~1.5-fold over mock) while isoform1 was similar to mock (Figure
233 5D). These data are consistent with only isoform2 acting as a transcription factor protein for *Hes5*
234 POU protein binding sequences. This assay was then repeated using the mutated isoform2 variants.
235 DsRed expression was normalized by POU6F2 and presented as a relative value compared to the

236 WT (Figure 5E). Transcriptional activity was reduced by 50% in the MT1 group (P=0.0334)
237 compared to WT. MT2 also showed decreased activity, but it was not statistically different from
238 the WT group (P=0.1367).

239 To complement the transcription factor binding assays, HDOCK was used to predict the
240 interaction of isoform2 with the two Hes5 POU binding sequences described above, 1) 5-
241 CCA$A_1A_2G_3C_4A_5A_6A_7T_8$-3', which also contains a three base pair 5' flank upstream (underlined
242 above) and a T>A substitution in the second position (A_2) relative to the OCT1 consensus; and 2)
243 5'-$A_1T_2G_3C_4T_5A_6A_7T_8$-3' which has an A>T substitution in the fifth position (T_5) relative to the
244 OCT1 consensus. HDOCK predicted a more favorable scoring function between isoform2 and the
245 Hes5 POU binding site 1(-340.48au) compared to site 2(-234.19au, respectively). For site 1, POU_S
246 docked onto sense 5'-$A_1A_2G_3C_4$-3' and POU_H onto antisense 3'-$T_5T_6T_7A_8$-5'; these interactions
247 are consistent with the literature(Zhou et al., 1996). Unlike the data obtained from the *in vitro*
248 transcription assay described above, SAMPDI (Supplementary Table 1) predicted that both MT1
249 and MT2 would impair DNA binding to site 1($\Delta\Delta G_{MT1}$=0.271; $\Delta\Delta G_{MT2}$=0.548 kcal mol^{-1}) or site
250 2 ($\Delta\Delta G_{MT1}$=0.261; $\Delta\Delta G_{MT2}$=0.254 kcal mol^{-1}), i.e. decrease the POU6F2-Hes5 binding affinity
251 for isoform2.
252
253 **Functional analysis of POU6F2 isoform1 as a potential transcription factor**
254 Compared to POU6F2 isoform2, the function of POU6F2 isoform1 is unclear. However, using the
255 Yeast One-Hybrid System with a 5'-upstream region of the porcine *Fshβ* as the bait sequence,
256 Yoshida et al. (Yoshida et al., 2014), cloned a cDNA encoding a partial sequence of the POU
257 domain from porcine pituitary. The clone was equivalent to POU6F2 isoform1 and was able to
258 modulate expression of developmental pituitary genes, using transient transfection assays of

promoter activity in CHO cells. We tested isoform1 against the predicted *Fshβ* protected site(5'-ATAAGCTTAAT-3'). Modeling showed that not only does isoform1 bind in the correct orientation (i.e., insert facing away from DNA) but the POU_S binds onto ATAA and POU_H onto TTAA, which agrees with the sites that POU6F1 monomer2 uses to bind CRH (crystal PDB code: 3D1N). Examining the *GnRH1* promoter we found a similar site but with 3 mismatches (AAAAGCATAGT, region of *GnRH1* promoter sequence that aligned with *Fshβ*). When we tested this site using HDOCK, isoform1 did not interact with the correct domains/orientation and the docking solutions were not in agreement with the binding mode predicted with *Fshβ*. However, we noticed that the *GnRH1* promoter region contains a reverse-complementary version of the POU6F2 consensus site with one A/T substitution (POU6F2 consensus: 5'-ATGCAAAT-3'; *GnRH1* site: 5'-TACGAAAA-3' = 3-ATGCTTTT-5', Figure 6A). Using 3D modeling, one sees the POU6F2 consensus site arrangement and appropriate binding for isoform1 (Figure 6B, i.e. POUs to ATGC half and POUh to AAAA half), which is in fact, in agreement with isoform2. The 44-nucleotide insert on isoform1 sticks away from the complex allowing it to bind. Next, DynaMut and CABS-flex were used to determine changes in protein structure that might be induced by MT1 and MT2 on isoform1 (Figure 6C and D). DynaMut predicted that MT1 destabilized while MT2 stabilized isoform1 folding ($\Delta\Delta_{GMT1}$=-0.562; $\Delta\Delta G_{MT2}$=1.728). CABS-flex revealed that isoform1 protein flexibility was decreased only with MT2 (P=0.0016).

To directly evaluate the transcriptional activity of WT and mutant isoform1 POU6F2 proteins, *in vitro* transcription assays were performed using a human GnRH cell line FNC-B4-hTERT(Hu et al., 2009). GnRH transcript was measured using qPCR. Isoform1 but not isoform2 was found to be expressed in FNC-B4-hTERT cells, whereas both isoforms were detected in human brain lysate, albeit isoform2 levels were drastically lower compared to isoform1

(Supplementary Figure 1). Further, expression of either WT-POU6F2 or MT2-POU6F2 isoform1 in these cells significantly decrease GnRH expression compared to mock (Mock=1; WT=0.7547±.014, ****P<0.0001; MT2=0.8458±0.032, **P<0.001; Figure 6E). No significant difference was found between WT and MT2 isoform1 treated groups (Figure 6E). Notably, MT1 significantly increased *GnRH1* transcript compared to both WT and MT2 groups (MT1=1.164±0.11, P<0.05 for both comparisons) but was not significantly different from the Mock group (Figure 6E). These experiments reveal that isoform1 POU6F2 proteins, transcriptionally regulate *GnRH1* (Figure 6F). Table 3. summarizes the *in vitro* experiments performed in this study.

DISCUSSION

Our findings demonstrate POU6F2 is necessary for human puberty and reproduction; they also reveal a novel action of POU6F2 isoform1 as a transcription factor capable of acting on the GnRH promotor. We present clinical and molecular genetics data from 15 patients who belonged to 12 independent families that highlighted POU6F2 variants. These patients all presented with pubertal failure and were diagnosed with IHH. Two of the POU6F2 mutations which would potentially alter DNA binding were then analyzed by molecular, cellular and bioinformatic techniques. These studies indicate that one of the POU domain mutations (MT1) alters the DNA binding capacity of both POU6F2 isoform1 and isoform2, and by extension, affects transcription efficiency. The lack of an effect by MT2 is consistent with new Turkish variome data(Kars et al., 2021) (unlike that in GnomAD), indicating that this mutation is probably too common in the Turkish population to cause IHH by itself, but may contribute to the phenotype in combination with other mutations.

Since IHH patients have low gonadotropins in the face of prepubertal serum sex steroid levels, the pathophysiology of this condition should reside in the pituitary and/or hypothalamus. POU6F2 has been shown to be highly expressed in the early embryonic pituitary and stimulate the expression of PROP1(Yoshida et al., 2014), though the specific isoforms were not examined. PROP1 is well known to induce POU1F1 and the development of gonadotropes and corticotropes in the anterior pituitary(Kioussi, Carriere, & Rosenfeld, 1999). POU1F1 also induces differentiation of GH, PRL, TSHB producing cell lineages in the anterior pituitary(Andersen & Rosenfeld, 2001) and when mutated, causes multiple pituitary hormone deficiency syndrome and hypopituitarism(Turton et al., 2005). However, it is unlikely that IHH in our patients is due to impaired pituitary effects of POU6F2 via PROP1 since our patients have only a deficiency of LH and FSH and not ACTH or any of the remaining three pituitary hormones (Growth hormone, Prolactin, and TSH) induced by POU1F1 subsequent to PROP1 stimulation.

There are many modulators of reproduction within the hypothalamus, but most are translated to the pituitary-gonadal axis via GnRH neurons and dysregulation of GnRH neurons prenatally or postnatally can result in an altered HPG axis. In this report we show that WT-POU6F2-isoform1 can directly inhibit *GnRH1* transcription and that MT1 alters the transcriptional activity of both isoform1 and 2. POU6F2 isoform2 in the POU domain region including the linker sequence has a high similarity with POU6F1. The recent crystallization of POU6F1 revealed that members of the POU6-family can bind target DNA as dimers such that the POU_S and POU_H domains of one monomer bind opposite faces of dsDNA via a flexible linker region, and that the POU_S domain of the other monomer binds adjacent to the first POU_S(Pereira & Kim, 2009). This is in contrast with PIT-1 (also known as POU1F1) which binds the same face of dsDNA as a dimer but shares features of OCT1 (also known as POU2F1) which binds opposite faces of dsDNA as either a monomer or

dimer(Herr & Cleary, 1995; Jacobson, Li, Leon-del-Rio, Rosenfeld, & Aggarwal, 1997; Reményi et al., 2001; Ryan & Rosenfeld, 1997). Since POU6F2 is the closest related clade member to POU6F1 and the fact that members of the same subclass of POU domain factors tend to have similar DNA-binding preferences(Andersen & Rosenfeld, 2001), it is expected that they bind DNA in a comparable manner. In fact, computational modeling found that isoform2 docked onto CRH in a manner identical to monomeric POU6F1, whereas isoform1 did not (Supplementary Table 1). To validate the HDOCK template-free binding benchmark, a simulation was run to test if the server could predict POU6F1 binding to CRH promoter from the individual structures and found that the prediction was in the exact same orientation as for the POU6F1-CRH co-crystal. The spatial arrangement in combination with overlapping interfacial contacts confirms that POU6F2 isoform2 is comparable to POU6F1 DNA binding to the CRH motif.

Computational modeling also found that isoform1 did not dock onto CRH in a manner identical to monomeric POU6F1. POU6F2 isoform1 was shown to interact with a region of the *FSHβ* promoter(Yoshida et al., 2014). Although a similar region (3 nucleotide changes) was found in the GnRH promoter, modeling did not show binding. However, an OCT1 consensus-like site(5'-ATGCTTTT-3') was identified in the human *GnRH1* promoter(-99 to -92). 3D modeling predicted that the POU_S bound to ATGC, and the POU_H inserted into a groove between both faces of the dsDNA, contacting both the TTTT and AAAA. Quantitative RT-PCR of *GnRH1* in a human cell line transfected with POU6F2 isoform1 showed exogenous expression of POU6F2 isoform1 decreased GnRH transcript levels confirming our 3D modeling.

Prenatally, GnRH cells migrate from the olfactory placode into the developing forebrain. Alterations in GNRH expression occur during migration with the cells pausing at the nasal forebrain junction(Duittoz et al., 2021). As they enter the forebrain, there is a significant increase in GnRH

transcription(Simonian & Herbison, 2001) with concomitant changes in protein expression(Kramer, Krishnamurthy, Mitchell, & Wray, 2000; Kramer & Wray, 2000) as well as neuronal activity(Duittoz et al., 2021). Previous studies in mouse showed that MSX and DLX, non-Hox homeodomain transcription factors, compete for same binding site and alter GnRH transcription differently, with DLX enhancing and MSX repressing GnRH expression(Givens et al., 2005). The authors reported that MSX mutant mice had more GnRH expressing cells at E13.5, yet the majority of these cells were confined to nasal regions being distributed in both expected regions as well as ectopically in the olfactory epithelium. In addition, the study reported that the mouse GN11 cell line, a model for immature migrating GnRH cells, expressed MSX while the GT1-7 cells, a model for mature mouse GnRH cells, expressed both DLX and MSX. The human cell line used for isoform1 assays in the present study is derived from olfactory mucosa, representing an immature GnRH cell. WT-POU6F2-isoform1 may thus have a role in maintaining low GnRH transcription levels specifically when GnRH cells are outside the forebrain, prioritizing migration over gene expression. This study suggests that mutations (such as MT1) releasing POU6F2 isoform1 repression would be detrimental to the developing GnRH neuronal system resulting in IHH.

In the adult, POU6F2 is expressed in the dorsal hypothalamus in a scattered fashion(Yoshida et al., 2014; Zhou et al., 1996), which may overlap with the dispersed location of GnRH neurons in the hypothalamus(Herbison, Porteous, Pape, Mora, & Hurst, 2008). Other POU domain genes(POU3F1 also known as OCT6(Wierman et al., 1997; Wolfe et al., 2002) and POU2F1 also known as OCT1(Leclerc & Boockfor, 2005)) have been shown to repress(Wierman et al., 1997) or enhance(Leclerc & Boockfor, 2005; Wolfe et al., 2002) *GNRH1* expression. Wierman et al(Wierman et al., 1997) speculated that POU3F1 is able to turn off and on the

373 transcriptional machinery in postnatal GnRH cells, influenced by the hormonal environment (such
374 as sex steroids), when groups of GnRH cells were reported to be unable to express the mature gene
375 product(King & Rubin, 1995). As an alternative/additional mechanism of disease via mechanisms
376 post-GnRH cell migration into the forebrain, the effects of POU6F2 variants to impair pubertal
377 development may occur indirectly to GnRH cells via the arcuate(infundibular) nucleus. The
378 arcuate kisspeptin neurons have been proposed as the hypothalamic GnRH pulse generator driving
379 fertility(Clarkson et al., 2017). Campbell et al. profiled gene expression in the arcuate nucleus of
380 the hypothalamus in adult mice and found *Pou6f2* is highly expressed with a subgroup of *Pomc*
381 neurons, a major anorectic gene, which may also give rise to kisspeptin neurons(Campbell et al.,
382 2017; Sanz et al., 2015). In addition, a single-cell transcriptome analysis of the hypothalamic
383 arcuate nucleus in E15 mouse showed that *Pou6f2* was one of the transcription factors showing
384 differential expression among subclusters(Huisman et al., 2019).

385 It is well recognized that allele specific expression(Kukurba et al., 2014) and/or alternative
386 splicing across tissues(Gutierrez-Arcelus et al., 2015) are important variables in determining the
387 disease-causing potential of a missense variant. Therefore, the impact of a variant is better
388 estimated by taking into consideration not only genome but also transcriptome data at the tissue
389 level(Li et al., 2017). Our study showed that a point mutation in a coding region can result in
390 missense mutant proteins across two isoforms due to splicing events. Considering the differential
391 ratio of *Pou6f2* isoforms in mouse tissues and primary GnRH cells themselves, investigating the
392 role of each isoform and the effect of mutations on their expression in relevant tissues is necessary
393 to unveil the pathogenic mechanism of POU6F2 in human IHH. This is particularly essential as
394 the central components of the HPG axis are among the least accessible tissues in human body. Our
395 *in silico* and *in vitro* assays of POU domain mutations, show that MT1 increased the generation of

isoform2 to isoform1 by altering splicing preference. This could have a profound effect on the GnRH cell subpopulation that predominantly expresses isoform1. If GnRH cells were now producing isoform2, new transcriptional targets could be impacted, disrupting the normal activity of downstream genes. Our experiments do not pinpoint whether it is this change in isoform1/isoform2 production and/or altered isoform1 activity that perturbs GnRH function *in vivo*. However, the defective function of isoform1 or a decreased amount of isoform1, could lead to increased GnRH1 transcription before migrating into the brain, and as such, directly cause the pathogenic effect as described above.

In contrast to MT1, MT2 did not change isoform preference in splicing nor did we see an impaired effect of MT2 isoform2 in our *in vitro Hes5* transcription assay that reached statistical significance. However, in this assay, the MT2 group was also not significantly different from the MT1 group(P=0.3519). Patients in Family-B and Family-C carry MT2, but both had additional variants in other genes. Patients in Family-B possessed a rare heterozygous variant in *CCDC141*, which encodes for a protein involved in embryonic GnRH neuron migration(Hutchins et al., 2016) and is a known IHH-causative gene(Turan et al., 2017). Thus, the co-occurrence of the rare variant in *CCDC141* may explain IHH in this kindred. The proband in Family-C had rare heterozygous variants in POU6F1. Although little is known about the significance of the site of the POU6F1 variants, it is possible that the combination of these variants in the closest paralogs to POU6F2 had an integrated effect to cause the IHH phenotype in this patient.

In summary, we provide evidence implicating variants in POU6F2 in the etiology of IHH with mutations in POU6F2 isoform1 directly impacting GnRH expression.

MATERIALS AND METHODS

Human experimental protocols were approved by either the Ethics Committee of the Cukurova University Faculty of Medicine and the institutional review board of the University of Mississippi Medical Center or by the Human Research Committee at the MGH, Boston, MA. All individuals and/or their legal guardians provided written informed consent. For experiments involving mice: All procedures were performed in accordance with National Institute of Neurological Disorders and Stroke (NIH/NINDS) IACUC animal ethics guidelines (ASP-1221-20).

Patients

Two large cohorts of IHH patients were screened for POU6F2 variants. The Cukurova cohort consisted of 416 IHH patients (nIHH, n=331 and KS, n=85) from 357 independent families recruited in Turkey. The Harvard Reproductive Endocrine Sciences Center's IHH cohort included 677 nIHH and 632 KS patients recruited nationally and internationally. Reproductive phenotypes suggestive of IHH was deemed present if they exhibited at least one of the following IHH-related phenotypes: micropenis or cryptorchidism (boys), absent puberty by age 13 in girls and by age 14 in boys, primary amenorrhea (girls), and/or a biochemical observation of hypogonadotropic hypogonadism. The KS patients additionally had anosmia/hyposmia as determined by self-reporting and/or physical examination by administering culturally appropriate formal or informal smell tests.

DNA sequencing and rare variant analyses

DNA samples for exome sequencing (ES) were prepared as an Illumina sequencing library, and in the second step, the sequencing libraries were enriched for the desired target using the Illumina Exome Enrichment protocol. The captured libraries were sequenced using Illumina HiSeq2000

Sequencer. The reads were mapped against UCSC (https://genome.ucsc.edu/cgi-bin/hgGateway) hg19. The variants in ES data were filtered against population polymorphism databases TR Variome(Kars et al., 2021) and gnomAD in the Cukurova cohort and against gnomAD in the Harvard cohort to obtain rare sequence variants (RSV), defined as variants with <0.001 minor allele frequency (MAF).The resulting RSVs were then screened for variants in *POU6F2* (NM_007252). The presence and segregation of significant variants within pedigrees were verified by Sanger sequencing on an Applied Biosystems PRISM 3130 auto sequencer. All animal procedures were approved by NINDS Animal Care and Use Committee and performed in accordance with NIH guidelines.

Expression of *Pou6f2* isoforms

Total RNA was extracted from mouse adult brain, pituitary, testis, and ovaries, using Trizol reagent (Invitrogen, 15596-026) according to manufacturer's instructions. Total RNA (1ug) was used for cDNA synthesis with oligo$(dT)_{16}$ primer and SuperScript III Reverse Transcriptase (Invitrogen, 18080-044) following the manufacturer's protocol. cDNAs from primary GnRH cells, generated as previously described(Kramer et al., 2000) were also analyzed. PCR analysis was performed using specific primers on *Pou6f2* exon8 (forward,5'-ACACAGACTCAGGTGGGACAA-3') and exon9 (reverse,5'-TTCCCGGTCGTAGTTTAG-CTT-3') or isoform2 specific primers (forward,5'-GCCATCTGCAGGTTTGAAA-3'; reverse,5'-CGTGTTGCTTTAAGCGTTTG-3') and products compared on 2% agarose gels.

***In vitro* splicing assay**

In silico splicing predictions for POU domain variants were performed using online applications (Human Splicing Finder (v3.1), NetGene2, RESCUE-ESE, and Splice Site Finder by Neural Network (SSFNN)). For *in vitro* splicing assay, a mini-gene system vector was constructed using the pSPL3 plasmid (provided by Dr. C.A.Stratakis, NICHD/NIH, USA). Exon11 and flanking intronic sequences (~300bp) of the *POU6F2* gene were amplified from human gDNA and inserted into the pSPL3. Mutant constructs were generated by site-directed mutagenesis(Reikofski & Tao, 1992). After sequencing confirmation, the plasmids were transfected into HEK293FT cells (Lipofectamine® LTX with PLUS™ reagent, Invitrogen). Cells were lysed 48hrs after transfection and total RNA extracted (Trizol Reagent). cDNA was synthesized from 1ug of RNA using oligo$(dT)_{16}$ primer and SuperScript III Reverse Transcriptase. PCR to amplify the splicing region of exon11 of the mini-gene constructs was performed using a forward primer (SD6, on exonA of pSPL3) and an exon11 specific reverse primer. The PCR fragments from mock, WT and two mutant vectors were compared on 2% agarose gel. The sequence of PCR products was confirmed with direct Sanger sequencing after TA cloning to isolate each fragment.

Molecular modeling

POU6F2 isoform1 and 2 were generated using C-I-TASSER(Zhang, Mortuza, He, Wang, & Zhang, 2018) from their amino acid sequences (UniProtKB codes: P78424-1 and P78424-2). Three-dimensional DNA structures were produced using w3DNA(Zheng, Lu, & Olson, 2009). POU6F2-DNA docking was simulated by HDOCK using template-free docking settings for the OCT1 DNA binding site(Yan, Tao, He, & Huang, 2020; Yan, Zhang, Zhou, Li, & Huang, 2017). As predicted POU6F2 isoform1 did not bind to this site. Since isoform1 was previously reported to bind to *Fshβ* (Yoshida et al., 2014), we tested isoform1 against the *Fshβ* protected site (5'-

ATAAGCTTAAT-3') and separately against an aligned site in the proximal promoter region of Gnrh1 (5'-AAAAGCATAGT-3'). Mutant proteins and folding free energy values for both isoforms were calculated by DynaMut(Rodrigues, Pires, & Ascher, 2018). Natural protein flexibility was detected using CABS-flex dynamics(Kuriata et al., 2018). WT vs mutant protein-DNA binding free energy values were predicted by SAMPDI(Peng, Sun, Jia, Li, & Alexov, 2018). All models were rendered using PyMOL molecular graphics software.

In vitro assay for isoform2 variants

The *Hes5* gene was previously reported to be upregulated by isoform2(Fiorino et al., 2016). Thus, *in vitro* transcription assays for human POU6F2 was performed using a reporter plasmid that encodes DsRed under a Hes5 promoter (Addgene, Cat# 26868). For POU6F2 expression vectors, cDNA was introduced into pcDNA3.1(+)-IRES-GFP plasmid. Isoform1 was synthesized (GeneArt) and isoform2 and two mutant plasmids were generated by site-directed mutagenesis PCR, deleting 108bp of exon11 and subsequently introducing the mutation(Ho, Hunt, Horton, Pullen, & Pease, 1989; Reikofski & Tao, 1992). Mock or POU6F2 plasmids were co-transfected with the Hes5p-DsRed reporter plasmid into HEK293FT cells. Total protein was harvested after 3 days of culture and analyzed by Western blot (mouse anti-DsRed, Clontech; rabbit anti-POU6F2, Invitrogen, PA5-35115). Band intensities were measured using ImageJ software to quantify expression.

In vitro assay for isoform1 variants

Since only isoform1 was found in GnRH cells, an *in vitro* assay for changes in GnRH expression was performed using a human GnRH cell line, FNC-B4-hTERT. 'FNC-B4' cells were first isolated

510 from fetal olfactory neuroepithelium(Romanelli et al., 2004). Telomerase-mediated
511 immortalization was performed on these cells, and the human GnRH cell line (FNC-B4-hTERT)
512 was established(Hu et al., 2009). Cells were grown in monolayer (37°C, 5%CO2) in F-12 Coon's
513 modification medium (Sigma, F6636) supplemented with Penicillin-Streptomycin (Gibco, 15140-
514 122) and 10%fetal bovine serum (Sigma, F7524). FNC-B4-hTERT cells were seeded into 6-well
515 plates and cultured until ~80% confluency. Cells were then transfected with mock (pcDNA-
516 3.1(+)_IRES-GFP), WT-POU6F2-isoform1, and two isoform1 mutant plasmids using FuGENE®
517 HD (Promega, E2311) following the manufacturer's instructions. Thirty-two hrs after transfection,
518 culture media were changed to serum free media for 16hrs prior to GnRH stimulation(Romanelli
519 et al., 2004). Cells were treated with GnRH (0.2uM,[D-Trp^6]-LH-RH, Sigma, L9761) for 3hrs and
520 harvested for RNA preparation. Experiments were performed in triplicate. Total RNA was
521 extracted using Trizol reagent. 250ng of total RNA of each group was reverse transcribed into
522 cDNA using 50uM oligo(dT)$_{20}$ and SuperScript III reverse transcriptase. All cDNA was stored at
523 -20°C until analysis of GnRH transcript levels using RT-qPCR. qPCR was performed with primers
524 specific for human Beta-Actin (*ACTB;* forward: 5'-CACCATTGGCAATGAGCGGTTC-3';
525 reverse, 5'-AGGTCT-TTGCGGATGTCCACGT-3') and GnRH (*GnRH1*; forward,5'-
526 CAACGCTTCGAATGCACCA-3'; reverse,5'-ATGTGCAACTTGGTGTAAGGATT-3'). The
527 primer efficiency of Beta-Actin was 92.3% with an R^2=0.9997. The primer efficiency of GnRH
528 was 126.71% with an R^2=0.9877, falling within a 'good' efficiency and amplification factor for
529 qPCR(Taylor, Wakem, Dijkman, Alsarraj, & Nguyen, 2010). qPCR was performed using
530 SsoAdvanced Universal SYBR® Green Supermix (BioRad, 1725271) and StepOne Real-Time
531 PCR System (Applied Biosystems). Samples amplified with the Beta-Actin primers were diluted
532 1:100. Samples amplified with GnRH primers were diluted 2:3. Each sample was run in triplicate.

Each group was run together on the qPCR machine which resulted in three unique runs. The average of all the automatic thresholds was taken and used to set a manual threshold. ΔΔCT was calculated to compare GnRH expression across treatment groups. This was done by first calculating the mean of the technical triplicates for each sample for each primer. The ΔCT was then calculated by taking the mean CT value for GnRH and subtracting the mean CT value for Beta-Actin for each sample. The ΔΔCT was calculated by subtracting the reference treatment condition (Mock) ΔCT from each of the ΔCT of the treatment conditions (WT, MT1 and MT2). Lastly, the relative expression of GnRH in each group was determined by taking 2 to the power of the negative ΔΔCT.

Statistical analysis

Data are expressed as mean± SEM, and statistical evaluation was performed using unpaired t tests (Prism for macOS, v9.3.1). Data from *in vitro* splicing assay and transcriptional assay was normalized and represented as relative compared to control or WT group. $P<0.05$ was considered statistically significant. For qPCR, the Mock ΔΔCT was set to 1 and the remaining treatment conditions were adjusted accordingly to compare across experimental runs. Statistical significance between group were compared using unpaired t tests across biological triplicates.

ACKNOWLEDGMENTS

We thank Dr. C.A. Stratakis (NICHD/NIH, USA) for providing the pSPL3 plasmid and Dr. Soo-Hyun Kim (St George's, University of London, United Kingdom) for providing FNC-B4-hTERT cells, Lacey Plummer for the data retrieval. This study was supported by University of Mississippi Medical Center, (grant DN00305, AKT), Cukurova University (scientific research project number 11364, AKT), National Institutes of Health, National Institute of Neurological Disorders and

Stroke (ZIANS-002824-30, SW), Eunice K. Shriver National Institute for Child Health and Human Development (P50HD104224-01, RB and SBS; R37 HD043341-19, R01 FD005712-04, SBS).

COMPETING INTERESTS

The authors declare no competing interests.

REFERENCES

Adzhubei, I. A., Schmidt, S., Peshkin, L., Ramensky, V. E., Gerasimova, A., Bork, P., . . . Sunyaev, S. R. (2010). A method and server for predicting damaging missense mutations. *Nat Methods, 7*(4), 248-249. doi:10.1038/nmeth0410-248

Andersen, B., & Rosenfeld, M. G. (2001). POU domain factors in the neuroendocrine system: lessons from developmental biology provide insights into human disease. *Endocr Rev, 22*(1), 2-35. doi:10.1210/edrv.22.1.0421

Bouilly, J., Messina, A., Papadakis, G., Cassatella, D., Xu, C., Acierno, J. S., . . . Pitteloud, N. (2018). DCC/NTN1 complex mutations in patients with congenital hypogonadotropic hypogonadism impair GnRH neuron development. *Hum Mol Genet, 27*(2), 359-372. doi:10.1093/hmg/ddx408

Campbell, J. N., Macosko, E. Z., Fenselau, H., Pers, T. H., Lyubetskaya, A., Tenen, D., . . . Tsai, L. T. (2017). A molecular census of arcuate hypothalamus and median eminence cell types. *Nat Neurosci, 20*(3), 484-496. doi:10.1038/nn.4495

Clarkson, J., Han, S. Y., Piet, R., McLennan, T., Kane, G. M., Ng, J., . . . Herbison, A. E. (2017). Definition of the hypothalamic GnRH pulse generator in mice. *Proc Natl Acad Sci U S A, 114*(47), E10216-E10223. doi:10.1073/pnas.1713897114

579 Duittoz, A. H., Forni, P. E., Giacobini, P., Golan, M., Mollard, P., Negrón, A. L., . . . Wray, S.
580 (2021). Development of the gonadotropin-releasing hormone system. *J Neuroendocrinol*,
581 e13087. doi:10.1111/jne.13087
582 Fiorino, A., Manenti, G., Gamba, B., Bucci, G., De Cecco, L., Sardella, M., . . . Perotti, D. (2016).
583 Retina-derived POU domain factor 1 coordinates expression of genes relevant to renal and
584 neuronal development. *Int J Biochem Cell Biol, 78*, 162-172.
585 doi:10.1016/j.biocel.2016.07.013
586 Givens, M. L., Rave-Harel, N., Goonewardena, V. D., Kurotani, R., Berdy, S. E., Swan, C. H., . .
587 . Mellon, P. L. (2005). Developmental regulation of gonadotropin-releasing hormone gene
588 expression by the MSX and DLX homeodomain protein families. *J Biol Chem, 280*(19),
589 19156-19165. doi:10.1074/jbc.M502004200
590 Gutierrez-Arcelus, M., Ongen, H., Lappalainen, T., Montgomery, S. B., Buil, A., Yurovsky, A., .
591 . . Dermitzakis, E. T. (2015). Tissue-specific effects of genetic and epigenetic variation on
592 gene regulation and splicing. *PLoS Genet, 11*(1), e1004958.
593 doi:10.1371/journal.pgen.1004958
594 Haddad, Y., Adam, V., & Heger, Z. (2020). Ten quick tips for homology modeling of high-
595 resolution protein 3D structures. *PLoS Comput Biol, 16*(4), e1007449.
596 doi:10.1371/journal.pcbi.1007449
597 Herbison, A. E., Porteous, R., Pape, J. R., Mora, J. M., & Hurst, P. R. (2008). Gonadotropin-
598 releasing hormone neuron requirements for puberty, ovulation, and fertility.
599 *Endocrinology, 149*(2), 597-604. doi:10.1210/en.2007-1139

600 Herr, W., & Cleary, M. A. (1995). The POU domain: versatility in transcriptional regulation by a
601 flexible two-in-one DNA-binding domain. *Genes Dev, 9*(14), 1679-1693.
602 doi:10.1101/gad.9.14.1679
603 Ho, S. N., Hunt, H. D., Horton, R. M., Pullen, J. K., & Pease, L. R. (1989). Site-directed
604 mutagenesis by overlap extension using the polymerase chain reaction. *Gene, 77*(1), 51-
605 59. doi:10.1016/0378-1119(89)90358-2
606 Howard, S. R., & Dunkel, L. (2019). Delayed Puberty-Phenotypic Diversity, Molecular Genetic
607 Mechanisms, and Recent Discoveries. *Endocr Rev, 40*(5), 1285-1317.
608 doi:10.1210/er.2018-00248
609 Hu, Y., Guimond, S. E., Travers, P., Cadman, S., Hohenester, E., Turnbull, J. E., . . . Bouloux, P.
610 M. (2009). Novel mechanisms of fibroblast growth factor receptor 1 regulation by
611 extracellular matrix protein anosmin-1. *J Biol Chem, 284*(43), 29905-29920.
612 doi:10.1074/jbc.M109.049155
613 Huisman, C., Cho, H., Brock, O., Lim, S. J., Youn, S. M., Park, Y., . . . Lee, J. W. (2019). Single
614 cell transcriptome analysis of developing arcuate nucleus neurons uncovers their key
615 developmental regulators. *Nat Commun, 10*(1), 3696. doi:10.1038/s41467-019-11667-y
616 Hutchins, B. I., Kotan, L. D., Taylor-Burds, C., Ozkan, Y., Cheng, P. J., Gurbuz, F., . . . Wray, S.
617 (2016). CCDC141 Mutation Identified in Anosmic Hypogonadotropic Hypogonadism
618 (Kallmann Syndrome) Alters GnRH Neuronal Migration. *Endocrinology, 157*(5), 1956-
619 1966. doi:10.1210/en.2015-1846
620 Jacobson, E. M., Li, P., Leon-del-Rio, A., Rosenfeld, M. G., & Aggarwal, A. K. (1997). Structure
621 of Pit-1 POU domain bound to DNA as a dimer: unexpected arrangement and flexibility.
622 *Genes Dev, 11*(2), 198-212. doi:10.1101/gad.11.2.198

623 Kars, M. E., Basak, A. N., Onat, O. E., Bilguvar, K., Choi, J., Itan, Y., . . . Ozcelik, T. (2021). The
624 genetic structure of the Turkish population reveals high levels of variation and admixture.
625 *Proc Natl Acad Sci U S A, 118*(36). doi:10.1073/pnas.2026076118
626 Kim, K. P., Han, D. W., Kim, J., & Schöler, H. R. (2021). Biological importance of OCT
627 transcription factors in reprogramming and development. *Exp Mol Med, 53*(6), 1018-1028.
628 doi:10.1038/s12276-021-00637-4
629 King, J. C., & Rubin, B. S. (1995). Dynamic alterations in luteinizing hormone-releasing hormone
630 (LHRH) neuronal cell bodies and terminals of adult rats. *Cell Mol Neurobiol, 15*(1), 89-
631 106. doi:10.1007/BF02069560
632 Kioussi, C., Carriere, C., & Rosenfeld, M. G. (1999). A model for the development of the
633 hypothalamic-pituitary axis: transcribing the hypophysis. *Mech Dev, 81*(1-2), 23-35.
634 doi:10.1016/s0925-4773(98)00229-9
635 Kramer, P. R., Krishnamurthy, R., Mitchell, P. J., & Wray, S. (2000). Transcription factor activator
636 protein-2 is required for continued luteinizing hormone-releasing hormone expression in
637 the forebrain of developing mice. *Endocrinology, 141*(5), 1823-1838.
638 doi:10.1210/endo.141.5.7452
639 Kramer, P. R., & Wray, S. (2000). Novel gene expressed in nasal region influences outgrowth of
640 olfactory axons and migration of luteinizing hormone-releasing hormone (LHRH) neurons.
641 *Genes Dev, 14*(14), 1824-1834.
642 Kukurba, K. R., Zhang, R., Li, X., Smith, K. S., Knowles, D. A., How Tan, M., . . . Montgomery,
643 S. B. (2014). Allelic expression of deleterious protein-coding variants across human
644 tissues. *PLoS Genet, 10*(5), e1004304. doi:10.1371/journal.pgen.1004304

645 Kumar, P., Henikoff, S., & Ng, P. C. (2009). Predicting the effects of coding non-synonymous
646 variants on protein function using the SIFT algorithm. *Nat Protoc, 4*(7), 1073-1081.
647 doi:10.1038/nprot.2009.86
648 Kuriata, A., Gierut, A. M., Oleniecki, T., Ciemny, M. P., Kolinski, A., Kurcinski, M., & Kmiecik,
649 S. (2018). CABS-flex 2.0: a web server for fast simulations of flexibility of protein
650 structures. *Nucleic Acids Res, 46*(W1), W338-W343. doi:10.1093/nar/gky356
651 Leclerc, G. M., & Boockfor, F. R. (2005). Identification of a novel OCT1 binding site that is
652 necessary for the elaboration of pulses of rat GnRH promoter activity. *Mol Cell Endocrinol,*
653 *245*(1-2), 86-92. doi:10.1016/j.mce.2005.10.026
654 Li, X., Kim, Y., Tsang, E. K., Davis, J. R., Damani, F. N., Chiang, C., . . . Montgomery, S. B.
655 (2017). The impact of rare variation on gene expression across tissues. *Nature, 550*(7675),
656 239-243. doi:10.1038/nature24267
657 Louden, E. D., Poch, A., Kim, H. G., Ben-Mahmoud, A., Kim, S. H., & Layman, L. C. (2021).
658 Genetics of hypogonadotropic Hypogonadism-Human and mouse genes, inheritance,
659 oligogenicity, and genetic counseling. *Mol Cell Endocrinol, 534*, 111334.
660 doi:10.1016/j.mce.2021.111334
661 Miao, Y., Li, C., Guo, J., Wang, H., Gong, L., Xie, W., & Zhang, Y. (2019). Identification of a
662 novel somatic mutation of POU6F2 by whole-genome sequencing in prolactinoma. *Mol*
663 *Genet Genomic Med, 7*(12), e1022. doi:10.1002/mgg3.1022
664 Peng, Y., Sun, L., Jia, Z., Li, L., & Alexov, E. (2018). Predicting protein-DNA binding free energy
665 change upon missense mutations using modified MM/PBSA approach: SAMPDI
666 webserver. *Bioinformatics, 34*(5), 779-786. doi:10.1093/bioinformatics/btx698

667 Pereira, J. H., & Kim, S. H. (2009). Structure of human Brn-5 transcription factor in complex with
668 CRH gene promoter. *J Struct Biol, 167*(2), 159-165. doi:10.1016/j.jsb.2009.05.003
669 Pitteloud, N., Hayes, F. J., Dwyer, A., Boepple, P. A., Lee, H., & Crowley, W. F., Jr. (2002).
670 Predictors of outcome of long-term GnRH therapy in men with idiopathic
671 hypogonadotropic hypogonadism. *J Clin Endocrinol Metab, 87*(9), 4128-4136.
672 doi:10.1210/jc.2002-020518
673 Reikofski, J., & Tao, B. Y. (1992). Polymerase chain reaction (PCR) techniques for site-directed
674 mutagenesis. *Biotechnol Adv, 10*(4), 535-547. doi:10.1016/0734-9750(92)91451-j
675 Reményi, A., Tomilin, A., Pohl, E., Lins, K., Philippsen, A., Reinbold, R., . . . Wilmanns, M.
676 (2001). Differential dimer activities of the transcription factor Oct-1 by DNA-induced
677 interface swapping. *Mol Cell, 8*(3), 569-580. doi:10.1016/s1097-2765(01)00336-7
678 Renault, C. H., Aksglaede, L., Wojdemann, D., Hansen, A. B., Jensen, R. B., & Juul, A. (2020).
679 Minipuberty of human infancy - A window of opportunity to evaluate hypogonadism and
680 differences of sex development? *Ann Pediatr Endocrinol Metab, 25*(2), 84-91.
681 doi:10.6065/apem.2040094.047
682 Richards, S., Aziz, N., Bale, S., Bick, D., Das, S., Gastier-Foster, J., . . . Committee, A. L. Q. A.
683 (2015). Standards and guidelines for the interpretation of sequence variants: a joint
684 consensus recommendation of the American College of Medical Genetics and Genomics
685 and the Association for Molecular Pathology. *Genet Med, 17*(5), 405-424.
686 doi:10.1038/gim.2015.30
687 Rodrigues, C. H., Pires, D. E., & Ascher, D. B. (2018). DynaMut: predicting the impact of
688 mutations on protein conformation, flexibility and stability. *Nucleic Acids Res, 46*(W1),
689 W350-W355. doi:10.1093/nar/gky300

690 Romanelli, R. G., Barni, T., Maggi, M., Luconi, M., Failli, P., Pezzatini, A., . . . Vannelli, G. B.
691 (2004). Expression and function of gonadotropin-releasing hormone (GnRH) receptor in
692 human olfactory GnRH-secreting neurons: an autocrine GnRH loop underlies neuronal
693 migration. *J Biol Chem, 279*(1), 117-126. doi:10.1074/jbc.M307955200
694 Ryan, A. K., & Rosenfeld, M. G. (1997). POU domain family values: flexibility, partnerships, and
695 developmental codes. *Genes Dev, 11*(10), 1207-1225. doi:10.1101/gad.11.10.1207
696 Saengkaew, T., Ruiz-Babot, G., David, A., Mancini, A., Mariniello, K., Cabrera, C. P., . . .
697 Howard, S. R. (2021). Whole exome sequencing identifies deleterious rare variants in
698 CCDC141 in familial self-limited delayed puberty. *NPJ Genom Med, 6*(1), 107.
699 doi:10.1038/s41525-021-00274-w
700 Sanz, E., Quintana, A., Deem, J. D., Steiner, R. A., Palmiter, R. D., & McKnight, G. S. (2015).
701 Fertility-regulating Kiss1 neurons arise from hypothalamic POMC-expressing progenitors.
702 *J Neurosci, 35*(14), 5549-5556. doi:10.1523/JNEUROSCI.3614-14.2015
703 Simonian, S. X., & Herbison, A. E. (2001). Regulation of gonadotropin-releasing hormone
704 (GnRH) gene expression during GnRH neuron migration in the mouse.
705 *Neuroendocrinology, 73*(3), 149-156. doi:10.1159/000054631
706 Strande, N. T., Riggs, E. R., Buchanan, A. H., Ceyhan-Birsoy, O., DiStefano, M., Dwight, S. S., .
707 . . Berg, J. S. (2017). Evaluating the Clinical Validity of Gene-Disease Associations: An
708 Evidence-Based Framework Developed by the Clinical Genome Resource. *Am J Hum*
709 *Genet, 100*(6), 895-906. doi:10.1016/j.ajhg.2017.04.015
710 Taylor, S., Wakem, M., Dijkman, G., Alsarraj, M., & Nguyen, M. (2010). A practical approach to
711 RT-qPCR-Publishing data that conform to the MIQE guidelines. *Methods, 50*(4), S1-5.
712 doi:10.1016/j.ymeth.2010.01.005

713 Teilum, K., Olsen, J. G., & Kragelund, B. B. (2011). Protein stability, flexibility and function.
714 *Biochim Biophys Acta, 1814*(8), 969-976. doi:10.1016/j.bbapap.2010.11.005
715 Turan, I., Hutchins, B. I., Hacihamdioglu, B., Kotan, L. D., Gurbuz, F., Ulubay, A., . . . Topaloglu,
716 A. K. (2017). CCDC141 Mutations in Idiopathic Hypogonadotropic Hypogonadism. *J Clin*
717 *Endocrinol Metab, 102*(6), 1816-1825. doi:10.1210/jc.2016-3391
718 Turton, J. P., Reynaud, R., Mehta, A., Torpiano, J., Saveanu, A., Woods, K. S., . . . Dattani, M. T.
719 (2005). Novel mutations within the POU1F1 gene associated with variable combined
720 pituitary hormone deficiency. *J Clin Endocrinol Metab, 90*(8), 4762-4770.
721 doi:10.1210/jc.2005-0570
722 Wierman, M. E., Xiong, X., Kepa, J. K., Spaulding, A. J., Jacobsen, B. M., Fang, Z., . . . Ojeda, S.
723 R. (1997). Repression of gonadotropin-releasing hormone promoter activity by the POU
724 homeodomain transcription factor SCIP/Oct-6/Tst-1: a regulatory mechanism of
725 phenotype expression? *Mol Cell Biol, 17*(3), 1652-1665. doi:10.1128/mcb.17.3.1652
726 Wolfe, A., Kim, H. H., Tobet, S., Stafford, D. E., & Radovick, S. (2002). Identification of a discrete
727 promoter region of the human GnRH gene that is sufficient for directing neuron-specific
728 expression: a role for POU homeodomain transcription factors. *Mol Endocrinol, 16*(3),
729 435-449. doi:10.1210/mend.16.3.0780
730 Xu, C., Messina, A., Somm, E., Miraoui, H., Kinnunen, T., Acierno, J., Jr., . . . Pitteloud, N. (2017).
731 KLB, encoding beta-Klotho, is mutated in patients with congenital hypogonadotropic
732 hypogonadism. *EMBO Mol Med, 9*(10), 1379-1397. doi:10.15252/emmm.201607376
733 Yan, Y., Tao, H., He, J., & Huang, S. Y. (2020). The HDOCK server for integrated protein-protein
734 docking. *Nat Protoc, 15*(5), 1829-1852. doi:10.1038/s41596-020-0312-x

735 Yan, Y., Zhang, D., Zhou, P., Li, B., & Huang, S. Y. (2017). HDOCK: a web server for protein-
736 protein and protein-DNA/RNA docking based on a hybrid strategy. *Nucleic Acids Res,*
737 *45*(W1), W365-W373. doi:10.1093/nar/gkx407
738 Yoshida, S., Ueharu, H., Higuchi, M., Horiguchi, K., Nishimura, N., Shibuya, S., . . . Kato, Y.
739 (2014). Molecular cloning of rat and porcine retina-derived POU domain factor 1
740 (POU6F2) from a pituitary cDNA library. *J Reprod Dev, 60*(4), 288-294.
741 doi:10.1262/jrd.2014-023
742 Zhang, C., Mortuza, S. M., He, B., Wang, Y., & Zhang, Y. (2018). Template-based and free
743 modeling of I-TASSER and QUARK pipelines using predicted contact maps in CASP12.
744 *Proteins, 86 Suppl 1*, 136-151. doi:10.1002/prot.25414
745 Zheng, G., Lu, X. J., & Olson, W. K. (2009). Web 3DNA--a web server for the analysis,
746 reconstruction, and visualization of three-dimensional nucleic-acid structures. *Nucleic*
747 *Acids Res, 37*(Web Server issue), W240-246. doi:10.1093/nar/gkp358
748 Zhou, H., Yoshioka, T., & Nathans, J. (1996). Retina-derived POU-domain factor-1: a complex
749 POU-domain gene implicated in the development of retinal ganglion and amacrine cells. *J*
750 *Neurosci, 16*(7), 2261-2274.
751 Zhu, J., Choa, R. E., Guo, M. H., Plummer, L., Buck, C., Palmert, M. R., . . . Chan, Y. M. (2015).
752 A shared genetic basis for self-limited delayed puberty and idiopathic hypogonadotropic
753 hypogonadism. *J Clin Endocrinol Metab, 100*(4), E646-654. doi:10.1210/jc.2015-1080

754

755

FIGURE LEGENDS

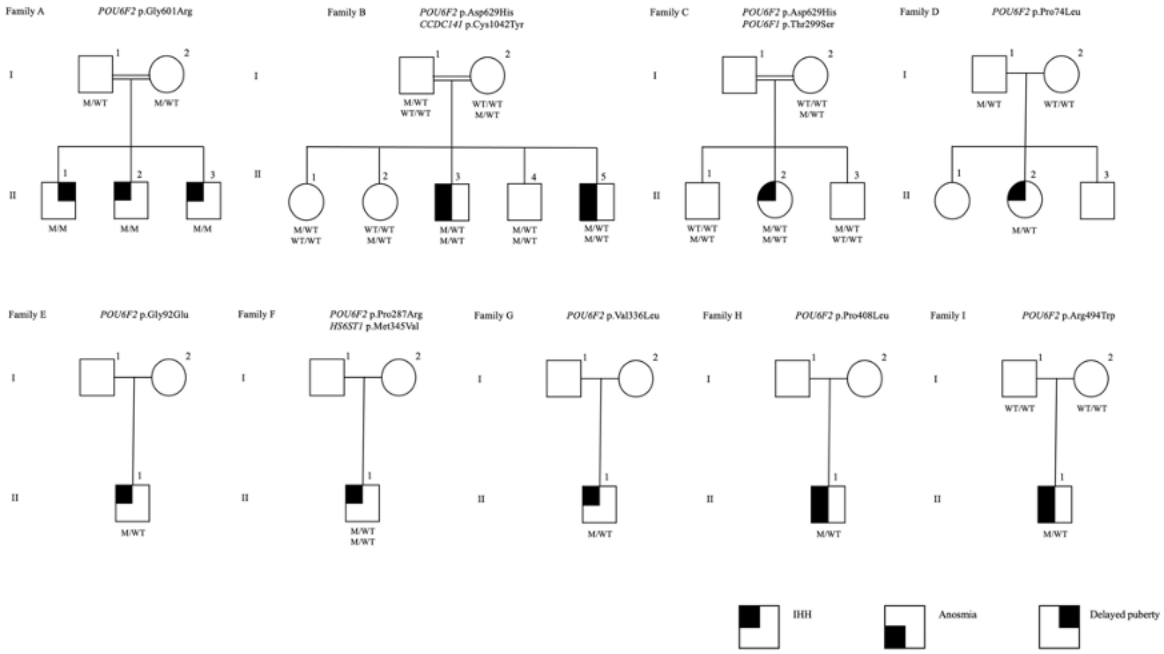

Figure 1. The pedigrees of the families with POU6F2 mutations. Affected males and females are represented by black squares and black circles respectively. White square symbols indicate unaffected male family members, white circle symbols represent unaffected female family members, and the double line indicates consanguinity. Under each symbol are the genotypes in the same order as the gene and variant descriptions, with WT and M denoting wild type and mutant, respectively. The legend denotes phenotypes as IHH, Anosmia, and Delayed puberty.

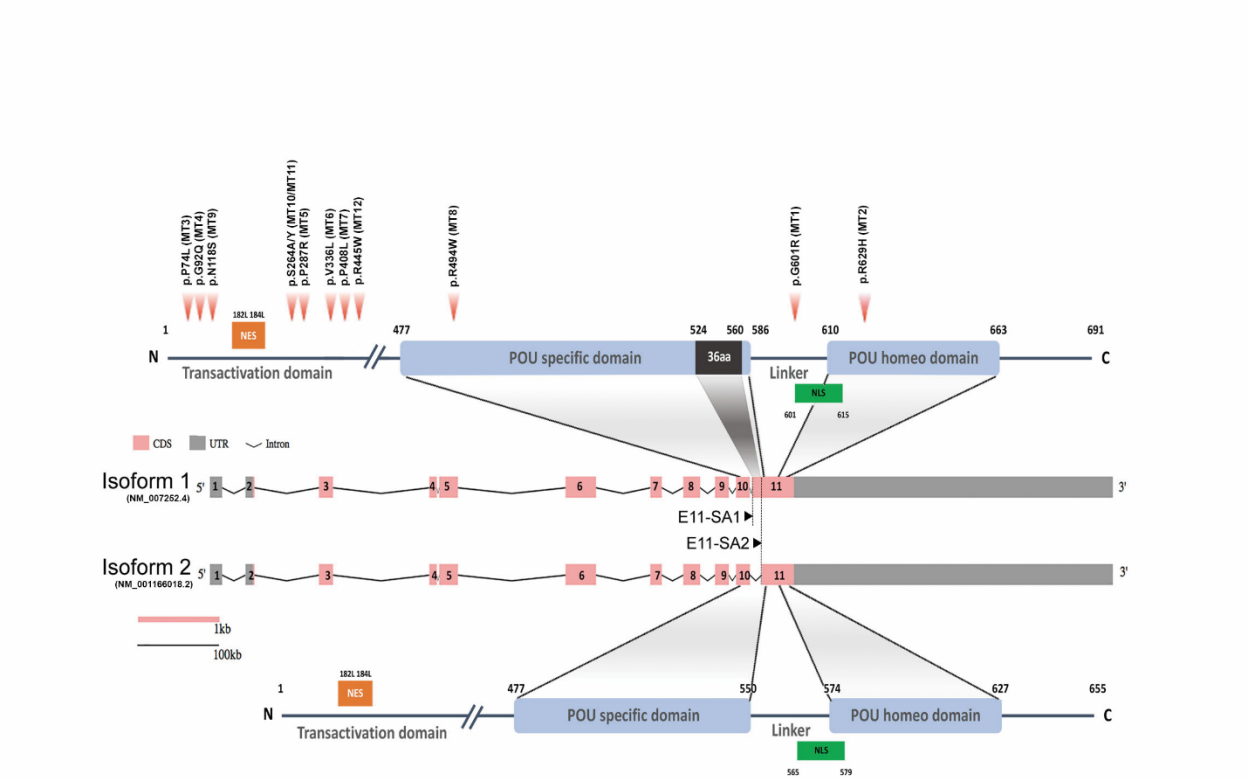

764

765 **Figure 2. Schematic diagram of human *POU6F2* isoforms.** Exon-intron structure of human
766 *POU6F2* isoforms (middle two schematics) drawn to scale using the Gene Structure Display
767 Server (GSDS 2.0, http://gsds.gao-lab.org). Exons are indicated by boxes to highlight the coding
768 sequence (CDS, pink) and untranslated region (UTR, gray). Introns are indicated by black lines
769 with a shrinked scale (0.01 ratio to scale of exons). Exon11 is alternatively spliced via two splicing
770 acceptor sites, E11-SA1 and E11-SA2, to generate isoform1 (upper schematic) and isoform2
771 (lower schematic), respectively. The two conserved DNA binding domains are indicated by blue
772 boxes and aligned to exons (encoded by exon10 to 11). Isoform1 has a unique 36aa insertion on
773 POU specific domain (black box) not found in any other POU protein family members. The amino
774 acid numbers are shown at the start and end point of functional domains. Twelve mutations
775 identified from IHH patients are indicated by red arrow heads (upper schematic). Mutation 1(MT1;
776 c.1801G>A, p.G601R in isoform1; c.1693G>A, p.G565R in isoform2) is in the linker region

777 between the two DNA binding domains. MT 2 (c.1885A>C, p.N629H in isoform1; c.1777A>C,
778 p.N593H in isoform2) is in the POU homeodomain. MT3-7, 9-12 are in the Transactivation
779 domain. MT8 (c.1480C>T, p.R494W) is in the POU-specific domain. Orange boxes; Nuclear
780 export signal (NES), green boxes; Nuclear localization signal (NLS).

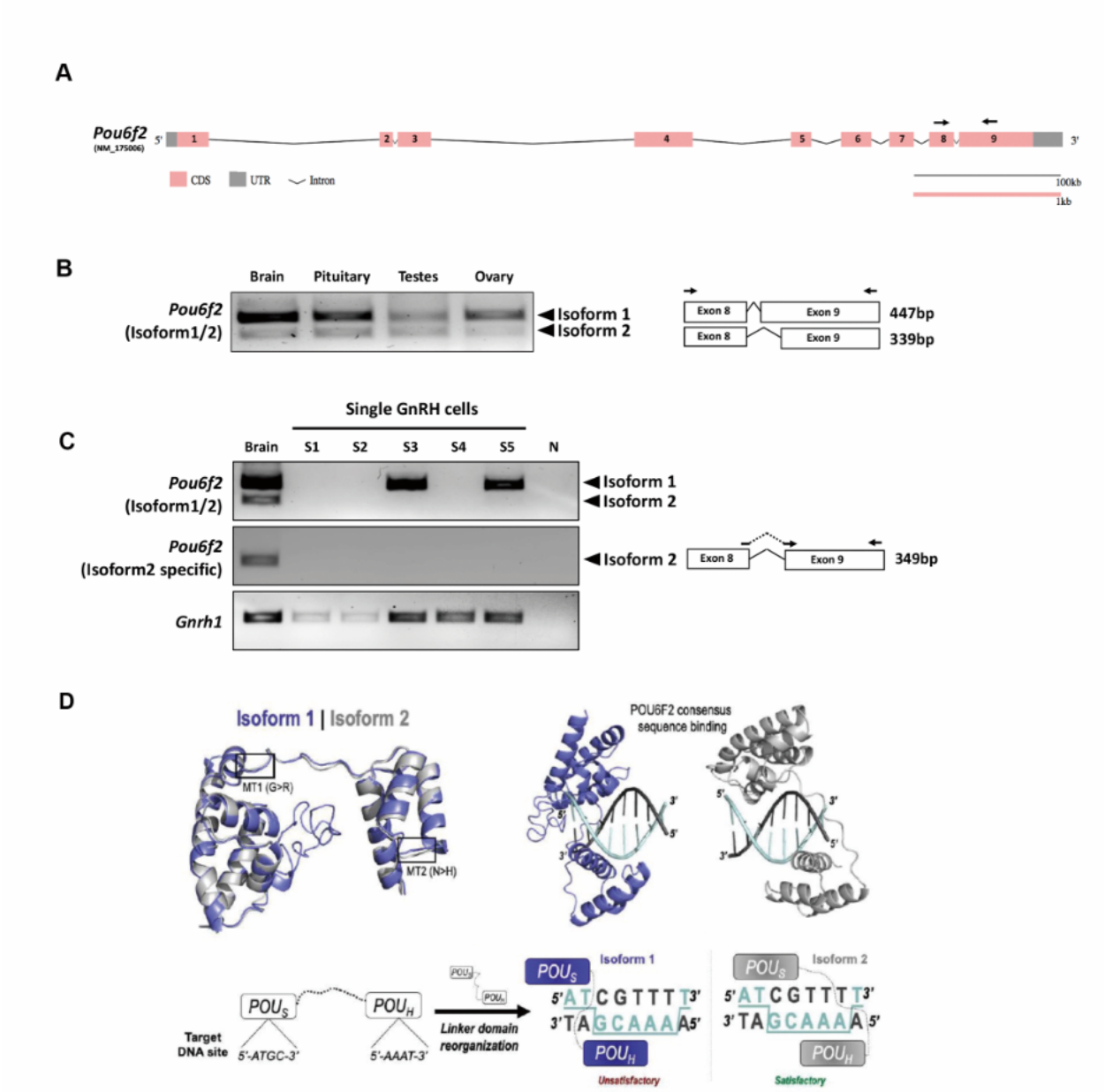

781

782 **Figure 3. Expression of *Pou6f2* isoforms in mouse and Bioinformatic prediction of POU6F2**
783 **isoforms bound to a DNA octamer. (A)** Exon-intron structure of mouse *Pou6f2* (GSDS 2.0,
784 http://gsds.gao-lab.org). In mice, only one isoform has been reported which is composed of 9 exons
785 and corresponds to isoform1 of human *POU6F2*. Primers used for PCR are shown as arrows on
786 exon8 and 9. **(B)** Gel image of RT-PCR analysis performed in mouse tissue. Top band (447 bp)

787 shows isoform1 and bottom band (339bp) shows isoform2 which is skipping 108bp by alternative
788 splicing on exon9. **(C)** Gel image of RT-PCR analysis of *Pou6f2* isoforms (top and middle gel) in
789 5 GnRH single cells (bottom gel). Only isoform1 was detected. **(D)** Upper Left, Superimposition
790 of isoform1 (purple) and 2 (gray) structures predicted by C-I-TASSER. The location of MT1 and
791 MT2 is indicated by boxes. Upper Right, HDOCK prediction of POU6F2 binding to the OCT1
792 DNA consensus site (5'-ATGCAAAT-3'). Template-free docking was used to prevent simulation
793 bias. Lower Left and Right, Structural representation of the interaction between each isoform and
794 dsDNA octamers. Two-dimensional cartoon illustrating the molecular interactions between each
795 POU domain and their predicted binding sites. Satisfactory (for isoform2) and unsatisfactory (for
796 isoform1) binding modes are indicated.
797
798 **Figure 3-source data B and C.** Raw images of uncropped and cropped gels from panels B and C
799 are included in the zipped source data as original tiffs and annotated pdf format.

A. *In silico* analysis through splice site prediction programs

	c.1801G>A (MT1)	c.1885A>C (MT2)
Human Splicing Finder (version 3.1)	Potential alteration of splicing (new acceptor site, new ESS site, ESE site broken)	Potential alteration of splicing (ESE site broken)
NetGene 2	Activating a new donor site (+17.14%)	Activating a new donor site (+12.85%)
RESCUE-ESE	new ESE site	ESE site broken
Splice Site Finder by Neural Net work (SSFNN)	No difference	No difference

ESE, exonic splicing enhancer; ESS, exonic splicing silencer

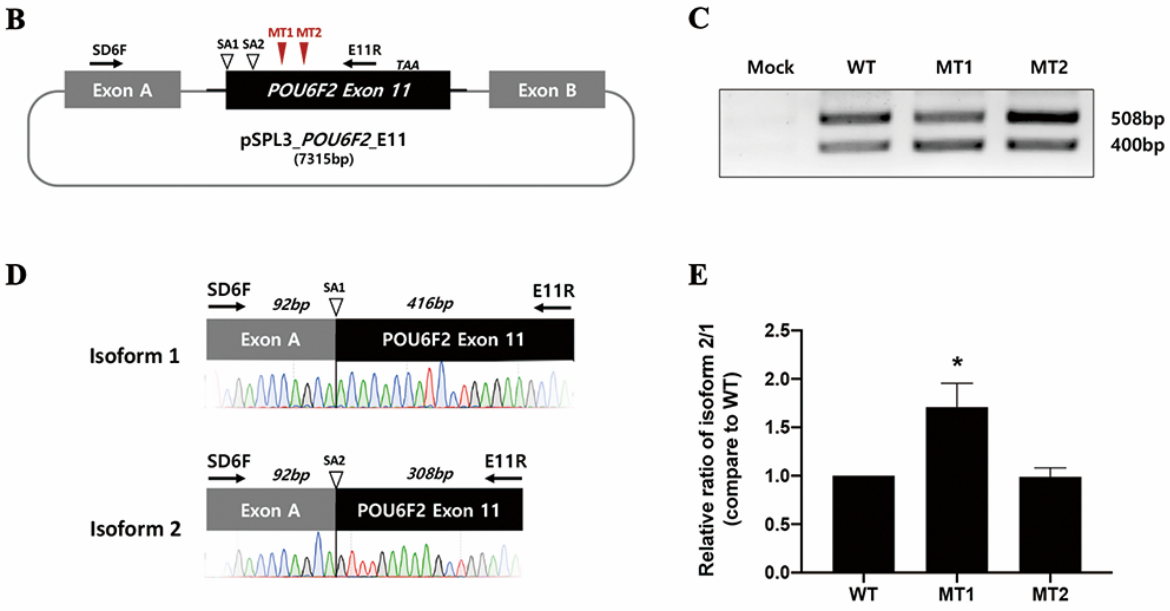

800

801 **Figure 4. *In silico* analysis of splice sites and the effect of MT1 or MT2 on isoform expression**
802 **using an *in vitro* splicing assay of human exon11. (A)** Table showing results of MT1 and MT2
803 on splice sites using *in silico* analysis. Three of the four programs predicted mutational changes**.**
804 **(B-E)** *In vitro* splicing assay of human POU6F2 exon11. **(B)** Exon11 of human *POU6F2* (Black
805 box) and flanking intronic sequences (~300bp, Black line) were inserted into pSPL3 minigene
806 vector which has two vectoral exons (ExonA and B, gray boxes). Splicing acceptor site for
807 isoform1 (SA1) and for isoform2 (SA2) are indicated by empty arrow heads. Two identified
808 mutations (red arrow heads) are located on the exon11 after SA2 splicing acceptor site and before

809 the stop codon (TAA). **(C)** RT-PCR using SD6F (forward primer on exonA) and E11R (Reverse
810 primer on POU6F2 exon11) resulted in two different sized bands (isoform1 and isoform2) in
811 assays using WT, MT1 and MT2. **(D)** Schematic diagram shows the amplified isoform1 and
812 isoform2 fragments from WT. Sequencing analysis confirmed the splicing junction from exonA
813 to SA1 (isoform1) and SA2 (isoform2). **(E)** Quantitative analysis of isoform1 and 2, from WT,
814 MT1 and MT2 constructs, performed via qPCR and represented as a relative isoform2/isoform1
815 ratio. MT1 increased isoform2 compared to WT (N=3). *P<0.05.
816
817 **Figure 4-source data C.** The zipped source data file contains raw images of the uncropped and
818 cropped gels from panel C (as original tiffs and annotated pdf format).

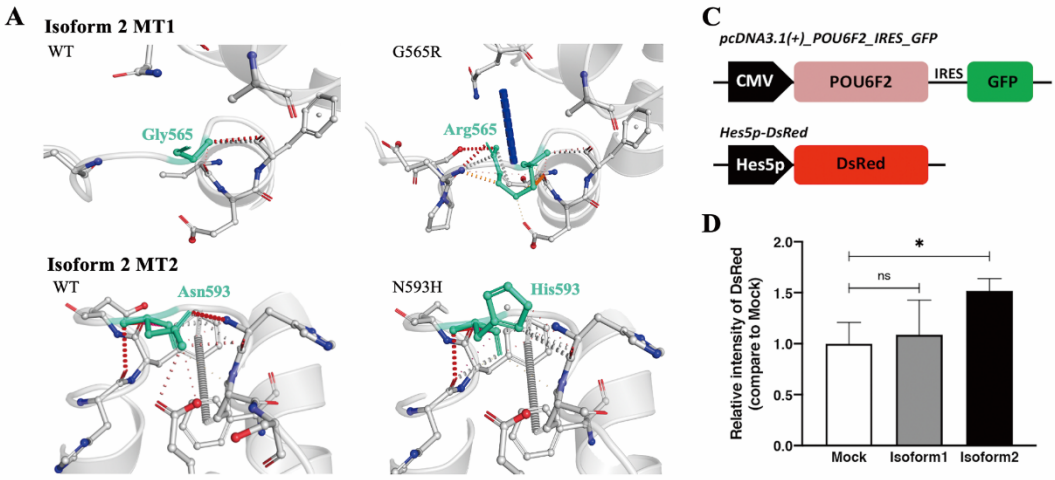

B

	Isoform 2 MT1 (G>R)	Isoform 2 MT2 (N>H)
DynaMut Folding free energy ΔΔG (kcal•mol^{-1})	0.956	0.211
SAMPDI Binding free energy ΔΔG (kcal•mol^{-1})	0.182	0.162
CABS-flex C_α Flexibility RMSF (Å)	p=0.0001	p=0.0001
Summary	Folding stabilized, DNA binding and flexibility impaired	Folding stabilized, DNA binding and flexibility impaired

SAMPDI:Positive values indicate destabilization of protein-DNA binding

Figure 5. Structural analysis of IHH mutations in POU6F2 isoform2 and *in vitro* transcription assay of human POU6F2 on *Hes5* promoter. (A) DynaMut prediction of WT and mutant proteins for isoform2. Individual amino acid substitutions are indicated in cyan. **(B)** Structural evaluation scores indicating how MT1 and MT2 affect POU6F2 isoform2 protein folding (DynaMut), natural protein flexibility (CABS-flex) and DNA binding (SAMPDI). DynaMut and CABS-flex represent changes in the individual protein structures, whereas SAMPDI represents changes in the affinity of POU6F2 to bind the OCT1 DNA consensus site ('5-ATGCAAAT-3'). Characterization of stabilizing or destabilizing effects are indicated. CABS-flex values analyzed using a paired-t test. **(C-E)** Transcriptional activity of POU6F2 isoforms were evaluated by *in vitro* transcription assay. **(C)** Schematic of vectors co-transfected into HEK293FT

cells. For POU6F2 expression vector, the CDS of each isoform was inserted into pcDNA3.1(+)_IRES-GFP after the CMV promoter. The reporter vector included the promoter sequences (~76bp) of *Hes5* followed by DsRed (Hes5p-DsRed**). (D)** After Western blot analysis using an anti-DsRed antibody, band intensities were measured (image J software) and represented as a relative value to that of the mock vector group (bar graph). Only isoform2 showed a significant increase in DsRed expression (~1.5 fold of mock). **(E)** Using the same assay, analysis for isoform2 mutations were performed. The band intensity of DsRed is normalized by POU6F2 intensity and compared to WT. The relative values are represented in the bar graph, showing that MT1 significantly decreased transcriptional activity (~0.5 fold of wild type). ns, not significant; **P* <0.05

Figure 5-source data D and E. The zipped source data file contains: 1) statistical data represented in panel D with and without normalization to WT control groups (pdf format), and 2) raw data and blots used for quantification from the Hes5 reporter assay (excel format).

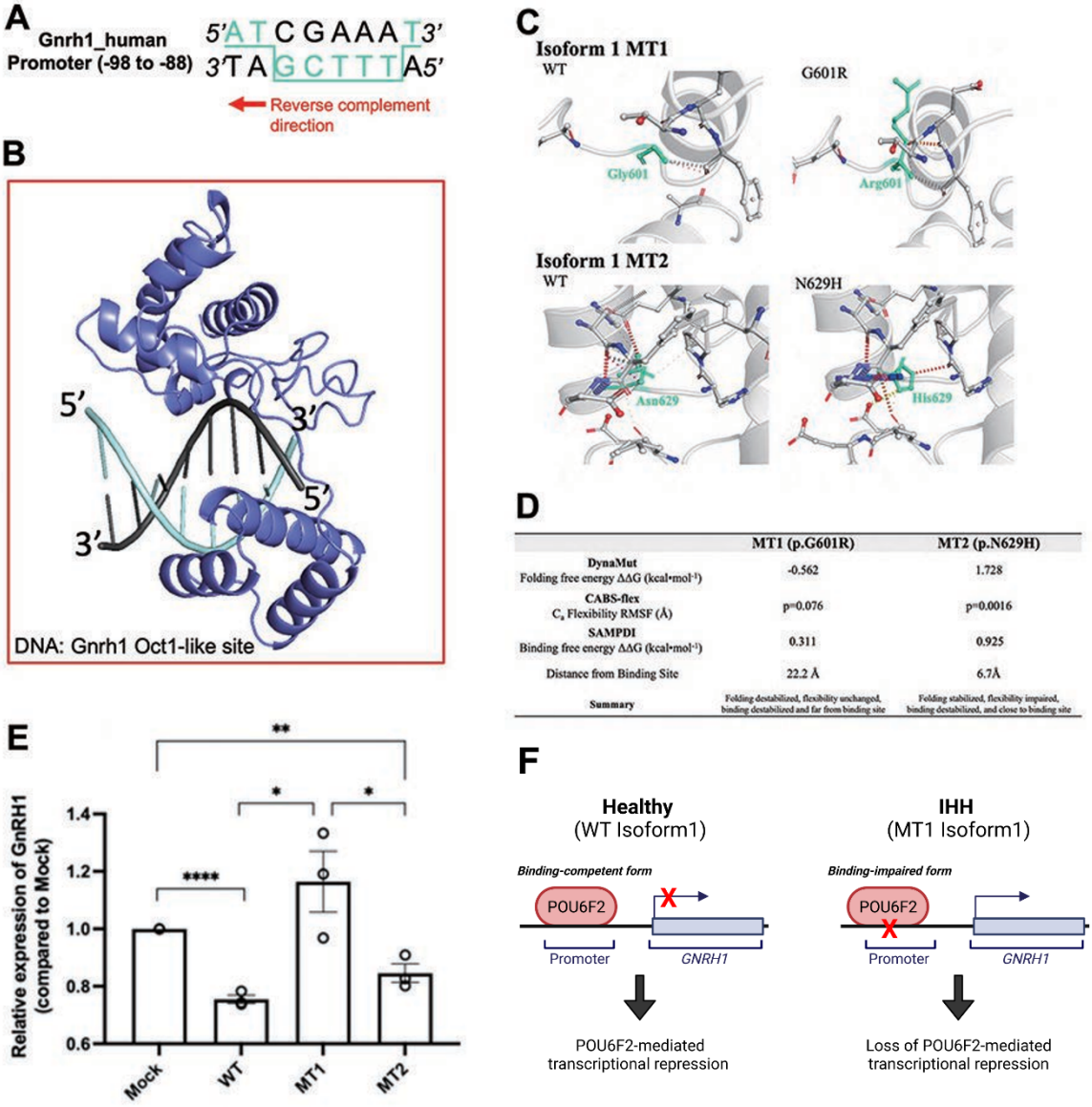

845

846 **Figure 6. Structural analysis of IHH mutations MT1 and MT2 on POU6F2 isoform1 and *in***
847 ***vitro* transcription assay of isoform1 in immortalized human GnRH cells. (A)** OCT1
848 consensus-like site (5'-ATGCTTTT-3') is identified in human *GnRH1* promoter (-98 to -88).

Binding site in 3D modeling uses POU_S to ATGC, and the POU_H is predicted to insert into a groove between both faces of the dsDNA, thus making contact with both TTTT and AAAA. **(B)** HDOCK prediction of POU6F2 isoform1 binding to the OCT1 consensus-like site. Template-free docking was used to prevent simulation bias. **(C)** DynaMut prediction of WT and mutant proteins for isoform1. Individual amino acid substitutions are indicated in cyan. **(D)** Structural evaluation scores indicating how MT1 and MT2 affect POU6F2 isoform1 protein folding (DynaMut), natural protein flexibility (CABS-flex) and DNA binding (SAMPDI). DynaMut and CABS-flex represent changes in the individual protein structures, whereas SAMPDI represents changes in the affinity of POU6F2 isoform1 to bind the OCT1 consensus-like site (5'-ATGCTTTT-3'). Characterization of stabilizing or destabilizing effects are indicated. CABS-flex values analyzed using a paired-t test. **(E)** Quantitative RT-PCR of *GnRH1* in FNC-B4-hTERT cells transfected by POU6F2 isoform1. The expression of *GnRH1* was normalized to each experimental mock group and the relative values are represented in the bar graph. MT1 significantly increased *GnRH1* transcript compared to both WT and MT2 groups but was not significantly different from the Mock group. **(F)** Schematic summary of isoform1 as a transcriptional regulator generated by Biorender (https://biorender.com/). Un-paired t test was performed (N=3), *P<0.05, **P<0.001, ****P<0.0001

Figure 6-source data E. The zipped source data file contains raw data from the RT-qPCR measurements presented in panel E (excel format).

869 **Table 1. Clinical characteristics of individuals with POU6F2 mutations.**

Family/individual no	Mutation	Age at diagnosis (year)	Sex	Ethnicity	Initial basal LH (mIU/mL) /Estradiol (ng/dL) or Testosterone (ng/dL)	Stimulated maximum LH (mIU/mL)	Olfaction	Reproductive phenotype
A II-1	p.Gly601Arg	15	M	Turkish	NA	NA	Normosmic	Delayed puberty, Constitutional delay in growth and puberty
A II-2	p.Gly601Arg	18	M	Turkish	NA	NA	Normosmic	Absent puberty, Infertility
A II-3	p.Gly601Arg	14	M	Turkish	0.14/<10	0.98	Normosmic	Absent puberty
B II-3	p.Asn629His	15	M	Turkish	<0.1/<10	3.3	Anosmic	Absent puberty, cryptorchidism
B II-5	p.Asn629His	0.5	M	Turkish	<0.1/<10	0.78	NA	Absent mini puberty, microphallus 1 cm, cryptorchidism
C II-2	p.Asn629His	17	F	Arabic	0.2/0.4	0.2	Normosmic	Absent puberty, primary amenorrhea
D II-2	p.Pro74Leu	16	F	Turkish	0.1/1.1	0.1	Normosmic	Absent puberty, primary amenorrhea
E II-1	p.Gly92Glu	16	M	Turkish	0.1/NA	<10	Normosmic	Absent puberty
F II-1	*p.Pro287Arg*	17	M	Turkish	<0.1/<12	3.6	Normosmic	Absent puberty
G II-1	p.Val336Leu	18	M	American Caucasian	NA	NA	Normosmic	Absent puberty
H II-1	p.Pro408Leu	18	M	American Caucasian	NA	NA	Anosmic	Absent puberty, cryptorchidism
I II-1	p.Arg494Trp	18	M	Ashkenazi Jew	NA	NA	Anosmic	Absent puberty
J II-1	p.Asn118Ser	20	M	Turkish	NA	NA	Normosmic	Absent puberty
K II-1	p.Ser264Ala p.Ser264Tyr	35	M	Ashkenazi Jew	NA	NA	Normosmic	Absent puberty
L II-1	p.Arg445Trp	18	M	Asian	NA	NA	Anosmic	Absent puberty, microphallus at birth, cryptorchidism

870

871 **Table 2. The molecular genetic characteristics of the *POU6F2* variants.**
872

Family /individual no	Variant name	Variant at cDNA level	Variant at protein level	TRV AC	TRV MAF	GnomAD MAF	CADD score	GERP	PP2	SIFT	ACMG/ AMP	Other IHH gene mutation /zygosity
A II-1, II-2, II-3	MT1	c.1801G>A	p.Gly601Arg	1 het /5170	0.000177	0.000017	28.8	5.28	D	D	VUS: PM1, PP2, PP3	None
B II-3, II-5	MT2	c.1885A>C	p.Asn629His	16 hets /6724	0.0023	0.000439	23.6	2.81	D	D	VUS: PM1, PP2, PP3	*CCDC141* p.Cys1042Tyr Het
C II-2	MT2	c.1885A>C	p.Asn629His	16 hets /6724	0.0023	0.000439	23.6	2.81	D	D	VUS: PM1, PP2, PP3	*POU6F1* p.Thr299Ser Het
D II-2	MT3	c.221C>T	p.Pro74Leu	0	0	0.000021	25.1	5.84	D	D	VUS: PP2	None
E II-1	MT4	c.275G>A	p.Gly92Glu	0	0	0.000007	27.8	5.84	D	D	LP: PM2, PP2, PP3	None
F II-1	MT5	c.860C>G	p.Pro287Arg	0	0	-	25.7	4.24	D	D	VUS: PM2, PP2	*HS6ST1* p.Met345Val Het
G II-1	MT6	c.1006G>C	p.Val336Leu	1 het /5174	0.000177	0.000027	23.8	6.17	D	T	VUS: PM1, PP2	None

H II-1	MT7	c.1223C>T	p.Pro408Leu	0	0	0.000011	31.0	5.62	D	D	LP: PM1, PM2, PP2, PP3	None
I II-1	MT8	c.1480C>T*	p.Arg494Trp	0	0	0.000020	34.0	5.48	D	D	VUS: PM1, PP2, PP3	None
J II-1	MT9	c.353A>G	p.Asn118Ser	0	0	-	19.9	5.02	T	D	VUS: PM1, PM2, PP2	None
K II-1	MT10	c.790T>G	p.Ser264Ala	0	0	0.000024	16.2	2.31	T	D	VUS: PM1, PM2, PP2	None
	MT11	c.791C>A	p.Ser264Tyr	0	0	0.000024	23.9	4.66	D	D	VUS: PM1, PM2, PP2	
L II-1	MT12	c.1333C>T	p.Arg445Trp	0	0	0.000032	26.7	5.70	D	D	VUS: PM1, PP2	None

Pro-to-Leu change at 74 (MT3) or 408 (MT7) could shift the hydrophilic/hydrophobic balance of this section of the protein toward hydrophobicity. Gly92 (MT4) is conserved in all the orthologs and most paralogs. This Gly-to-Glu mutation, which is predicted likely pathogenic, could add a strong ionic charge that is normally absent in its vicinity. Pro287(MT5) is embedded in a short Proline-rich region, which is well conserved. Mutations in this region have been implicated in prolactinoma (p.Pro280Leu and Gly292Ser) and Wilms tumor susceptibility (p.Ser270Pro and p.Pro273Leu) (Miao et al., 2019). Val336 (MT6) is well conserved in orthologs and partly conserved in paralogs. This Val-to-Leu mutation is an amino acid substitution in the same hydrophobic group, so it's predicted as a tolerant variation from the SIFT but still deleterious from PP2 prediction.

Abbreviations: Het, heterozygous; AC, allele count; MAF, minor allele frequency; TRV, Turkish Variome; GnomAD, The Genome Aggregation Consortium; InterVar, Interpretation of genetic variants by the ACMG/AMP 2015; VUS, variant uncertain significance;

LP, likely pathogenic; PM, pathogenic moderate; PP, pathogenic supporting; CADD, Combined Annotation Dependent Depletion; GERP, Genomic Evolutionary Rate Profiling. Variants are described according to the RefSeq numbers following the gene names: *POU6F2*, NM_007252; *CCDC141*, NM_173648; *POU6F1*, NM_001330422; *HS6ST1*, NM_004807. PolyPhen-2, Polymorphism Phenotyping v2; SIFT, Sorting Intolerant From Tolerant; D, deleterious; T, tolerated.

* A *de novo* mutation.

889 **Table 3. Summary of *in vitro* experiments**

890

	Expression in primary mouse GnRH neurons (Fig3)	**Exon11 Splicing assay in minigene Transfected HEK293 cells (Fig4)**			**in vitro transcription assays using a DsRed reporter under the Hes5 promoter in HEK293 cells (Fig5)**			**Isoform1 *in vitro* transcription assays in human GnRH cell line FNC-B4-hTERT (Fig6)**		
		WT	MT1	MT2	WT	MT1	MT2	WT	MT1	MT2
POU6F2 Isoform1	Present	Normal	Decreased or normal	Normal	Normal	Not Assayed	Not Assayed	Decreased	Increased	Decreased
POU6F2 Isoform2	Absent	Normal	Increased	Normal	Increased	Decreased	Decreased but ns	Not Assayed	Not Assayed	Not Assayed

SUPPLEMENTARY FIGURES AND TABLES

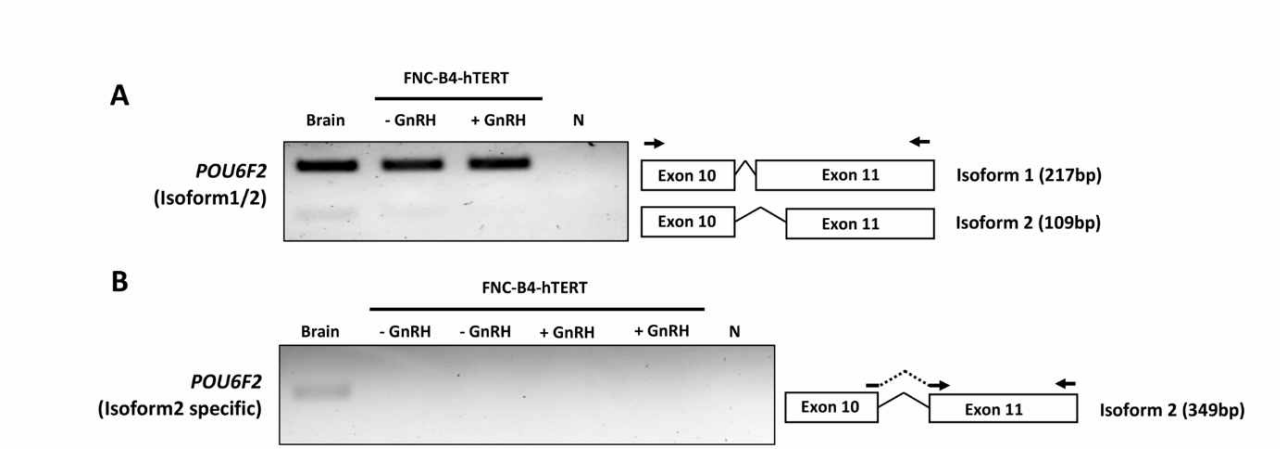

Supplementary Figure 1. Expression of *POU6F2* isoforms in human brain and FNC-B4-hTERT cells. (A) RT-PCR analysis performed in human brain and immortalized GnRH cells (with or without GnRH stimulation). Top band (217 bp) shows isoform1 and bottom band (109bp) shows isoform2 which is skipping 108bp by alternative splicing on exon 11. Primers used for PCR are shown as arrows on exon 10 and 11. **(B)** RT-PCR analysis performed using isoform2 specific primers (shown as arrows on the junction of exon 10-11 and exon 11). Isoform2 (349bp) was detected in human brain but not in FNC-B4-hTERT cells.

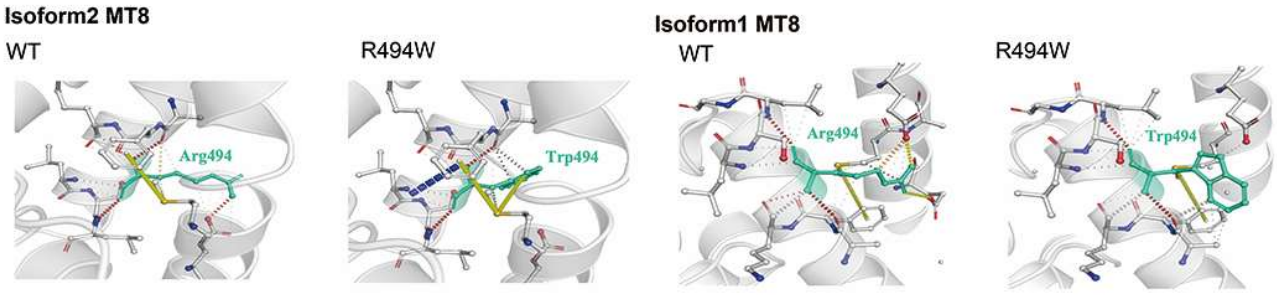

	Isoform 2 MT8 (R>W)
DynaMut Folding free energy ΔΔG (kcal•mol^{-1})	0.029
CABS-flex C_a Flexibility RMSF (Å)	p=0.0877
Distance from Binding Site	20.9 Å
Summary	Folding stabilized, DNA binding impaired, flexibility unchanged, and very far from binding site

	Isoform 1 MT8 (R>W)
DynaMut Folding free energy ΔΔG (kcal•mol^{-1})	-0.039
CABS-flex C_a Flexibility RMSF (Å)	p=0.0018
Distance from Binding Site	20.5 Å
Summary	Folding destabilized, flexibility impaired, binding destabilized, and very far from binding site

Supplemental Figure 2. Structural analysis of IHH mutation MT8 into POU6F2 isoform1 and 2. Structural evaluation scores indicating how MT8 affects POU6F2 isoform1 and isoform2 protein folding (DynaMut) and natural protein flexibility (CABS-flex) in the individual protein structures. Characterization of stabilizing or destabilizing effects are indicated. CABS-flex values analyzed using a paired-t test.

Supplemental Table 1. Computational analysis of variants bound to DNA targets

POU6F2		Hes5 site 1	Hes5 site 2	CRH promoter	Oct1 site	FSH site	Gnrh1 site
Isoform	Mutation	*5'-CCAAAGCAAAT-3'*	*5'-ATGCTAAT-3'*	*5'-AGCATAAATAATAA-3'*	*5'-ATGCAAAT-3' (POU6F2 Iso2 site)*	*5'-ATAAGCTTAAT-3' (CRH-like site)*	*5'-AAAAGCATAGT-3' (Oct1-like site)*
Isoform 1	MT1	----------Incorrect binding Predicted ----------				0.068	0.311
	MT2					0.459	0.925
	MT8					0.322	0.815
Isoform 2	MT1	0.271	0.261	0.233	0.182		
	MT2	0.548	0.254	0.316	0.162		
	MT8	0.609	0.841	0.870	0.729		

Binding free energy ($\Delta\Delta G$, kcal mol^{-1}) is predicted using SAMPDI and represented in the table.
Positive values indicate **destabilization** of protein-DNA.